國 立 交 通 大 學

電子工程學系 電子研究所碩士班

碩 士 論 文

IEEE 802.16a 分時雙工正交分頻多重進接之

下行通道估測之研究與技術

Study and Techniques of IEEE 802.16a TDD

OFDMA Downlink Channel Estimation

研 究 生：陳盈縈

指導教授：林大衛 博士

中 華 民 國 九 十 三 年 六 月

IEEE 802.16a 分時雙工正交分頻多重進接之下行通道估測之研究與技術

Study and Techniques of IEEE 802.16a TDD OFDMA Downlink Channel Estimation

研究生: 陳盈縈　　Student: Ying-Ying Chen

指導教授: 林大衛 博士　　Advisor: Dr. David W. Lin

國 立 交 通 大 學

電子工程學系　電子研究所碩士班

碩士論文

A Thesis

Submitted to Department of Electronics Engineering & Institute of Electronics
College of Electrical Engineering and Computer Science
National Chiao Tung University
in Partial Fulfillment of Requirements
for the Degree of
Master
in
Electronics Engineering
June 2004
Hsinchu, Taiwan, Republic of China

中華民國九十三年六月

IEEE 802.16a 分時雙工正交分頻多重進接之下行通道估測之研究與技術

研究生：陳盈縈　　指導教授：林大衛 博士

國立交通大學

電子工程學系 電子研究所碩士班

摘要

正交分頻技術近來因為能在行動環境中穩定高速傳輸而廣受注目，IEEE 802.16a即是一個基於正交分頻多重進接技術用於無線區域網路和大都會網路的標準。

本論文主要在討論 IEEE 802.16a 下行通道估測中的兩個重點:內插的技巧以及使用時域的資料來做改善的方法。

我們使用最小平方差的估測器來估計在導訊上的通道頻率響應而不用線性平均最小平方差的估測器，除了因為硬體的計算方便，也因為我們不知道通道的統計特性而不能使用線性平均最小平方差的估測器。而內插的方法我們則研究了線性內插，二次式內插以其三次樣條函數內插（cubic spline）。而在用時域的資料改善的方法有下列四種：移動平均 (moving average)，指數平均 (exponential average)，最小平均平方差適應 (LMS adaptation）以其二維內插法。

我們的在靜態以及瑞雷通道上模擬，在靜態通道上時，當雜訊比高於 24 分貝時，二維的內插法有最好的表現。而當雜訊比小於 24 分貝時，最小平均平方差適應的方法最好。

因為在瑞雷通道時通道的變化，我們所提出的方法需要做一些修改。而在瑞雷通道上的模擬則也是二維的內插法有最好的表現。當接收者時速 27 公里時，二維內插法加上使用四組可變導訊的效果最佳，且在二維內插時若再頻率域使用二次內插也會有較佳的結果。而這個結果與理想的結果相差約十分貝左右。

Study and Techniques of IEEE 802.16a TDD OFDMA Downlink Channel Estimation

Student: Ying-Ying Chen Advisor: Dr. David W. Lin

Department of Electronics Engineering
& Institute of Electronics
National Chiao Tung University

Abstract

OFDM (orthogonal frequency division multiplexing) technique has drawn much interest recently for its robustness in the mobile transmission environment and its high transmission data rate. IEEE 802.16a is a wireless local and metropolitan area networks standard which is based on OFDMA (orthogonal frequency division multiple access) technique.

This work considers two main subjects of the downlink channel estimation under the specifications of IEEE 802.16a, the interpolation schemes and the time-domain improvement techniques.

We use LS instead of LMMS estimator for estimations of pilot carriers, not only because we do not know the statistical properties of channels but also for its low computational complexity. We study the linear, the second-order and the cubic spline interpolations. And the 4 kinds of time-domain improvement skills are the moving average, exponential average, the LMS adaptation, and the two-D interpolation.

We did the simulation on both static and Rayleigh fading channels. In the static channel, the two-D interpolation performs the best when E_b/N_0 > 24dB; meanwhile, the LMS adaptation technique has the best performance when E_b/N_0 < 24dB.

In the Rayleigh fading channel, due to the change of the channel impulse response, the time-domain improvement skills mentioned above need to be modified.

When the speed of the vehicle is 27 km/h, the two-dimensional interpolation with four sets of variable location pilots and with second-order interpolation on the frequency domain can estimate the channel best and is about 10 dB worse than the ideal one.

誌謝

這篇論文能夠順利完成，最要感謝的人是我的指導教授 林大衛 博士。謝謝老師在兩年的研究所生涯中給我的指導與教誨，在此對老師獻上最大的感激之意。

此外，感謝實驗室中所有的成員，包含各位師長、同學、學長姐與學弟妹們。我要感謝吳俊榮學長、崑健肥學長與林郁男學長給予我在研究過程上的指導與建議，還有宗書、筱晴、明哲、馬克、長毛、仰哲、岳賢等同學與我彼此勉勵、互相討論，讓我這兩年的生活中充滿了快樂的回憶。

我也要感謝我的父母、妹妹及其他的朋友，不論我在失意或是開心的時候，都能分擔分享我的心情。

還有我的男友小賴，在這兩年與我一起努力獲得碩士學位，當我的出氣筒，培養我的 EQ，感恩啦！

最後，我要感謝校門口的土地公伯伯，謝謝你終於讓我順利畢業了，將要踏入一段新的生涯，我會繼續加油的，耶!

誌於 2004.7 風城交大

盈縈

Contents

List of Figures

List of Tables

Chapter 1

Introduction

Because the demand for high data rate wireless communications grows rapidly recently, orthogonal frequency division multiplexing (OFDM) has been studied widely in wireless communications due to its high transmission capability with high bandwith efficiency and its robustness to multipath delay.

OFDM system transmits data using a set of parallel low bandwidth subcarriers. The subcarriers are independent from each other even though their spectra overlap, which results in its bandwidth efficiency and resistance to the ICI (inter-carrier-interference) effect. And due to the low bandwidth of subcarriers, each subcarrier can resist worse channel whose coherence bandwidth is smaller. That is, subcarriers can suffer longer delay spread, thus ISI (inter-symbol-interference) is also reduced. High data rate systems are also achieved by using a large number of carriers. OFDM can be easily generated using an inverse fast Fourier transform (IFFT) and received using a fast Fourier transform (FFT).

It is also a technique that can achieve the spectral efficiency requirements and the high data capacity at the same time, so it has been commonly used in wireless LAN stantards such as the IEEE802.11 series, the European HIPERLAN/2, the Japanese Multimedia Mobile Access Communications [1], Digital Audio Broadcasting (DAB) and Digital Video Broadcasting (DVB) in Europe and Australia [2], [3]. In this thesis, we consider the IEEE 802.16a [4] WirelessMAN OFDMA system, which specifies the air interface of

fixed (stationary) broadband wireless access systems providing multiple access, but we consider its use and performance also in mobile wireless communication. And we focus on the downlink channel estimation. There are two major items of work done in the thesis: the different schemes of interpolations to estimate the channel frequency response on data carriers, and the time-domain improvement skills to use the information of other symbols for better estimations.

This thesis is organized as follows. First, we introduce the concepts of OFDM and OFDMA in chapter 2. And the standard IEEE 802.16a, as our system is based on, is introduced in chapter 3. In chapter 4, the channel estimation algorithm for downlink transmission is discussed. The different interpolation schemes and time-domain improvement methods are also introduced in chapter 4. Chapter 5 presents the simulation results based on the algorithm in chapter 4. Finally, conclusions and future works are given in chapter 6.

Chapter 2

Overview of OFDM and OFDMA

2.1 OFDM

The material in this chapter is largely taken from [5], [6], and[7].

2.1.1 Concept and brief mathematical expression of OFDM

In a single carrier system, a single fade or interference can cause the entire link to fail, but in a multicarrier system, only a small percentage of subcarriers will be affected. Error correction coding can then be used to correct for the few erroneous subcarriers. And OFDM is a special case of multicarrier transmission.

In a classical parallel data system, the total signal frequency band is divided into non-overlapping frequency channels. It seems good to avoid spectral overlap of channels to eliminate inter-channel interference. However, this leads to inefficient use of the available spectrum. To cope with the inefficiency, the concept of using parallel data transmission by means of frequency division multiplexing (FDM) was published in mid-1960s. The concept of FDM was to use parallel data streams with overlapping carriers. The basic idea of OFDM is to divide the available spectrum into several subchannels (subcarriers). By making all subchannels narrowband, they experience almost flat fading, which makes equalization and channel estimation easier. To obtain a high spectral efficiency, the frequency response of the subchannels are overlapping and orthogonal, hence the name OFDM. This orthogonality can be completely maintained, even though the signal passes

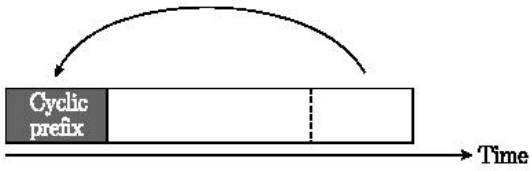

Fig. 2.1: The cyclic prefix is a copy of the last part of the OFDM symbol.

through a time-dispersive channel, by introducting a cyclic prefix. A cyclic prefix is a copy of the last part of the OFDM symbol which is prepended to the transmitted symbol, see Figure 2.1. This makes the transmitted signal periodic, which plays an important roll in avoiding intersymbol and intercarrier interference [8]. Although the cyclic prefix introduces a loss in signal-to-noise ration (SNR), it is usually a small price to pay to mitigate interference. For this system we employ the following assumptions:

- The channel impulse response is shorter than the cyclic prefix.
- Transmitter and receiver are perfectly synchronized.
- The fading is slow enough for the channel to be considered constatn during one OFDM symbol interval.
- Channel noise is additive, white, and complex Gaussian.

The brief mathematical description of the OFDM system allows us to see how the signal is generated. Mathematically, each carrier can be described as a complex wave:

$$S_c(t) = A_c(t)e^{j[w_c t+\phi_c(t)]}. \tag{2.1}$$

The real signal is the real part of $s_c(t)$. Both $A_c(t)$ and $\phi_c(t)$, the amplitude and phase of one carrier, can vary on a symbol-by-symbol basis. But the values of the parameters are constant over the symbol duration τ.

An OFDM signal consists of many carriers. Thus the complex signal $S_s(t)$ can be represented as:

$$S_s(t) = \frac{1}{N}\sum_{n=0}^{N-1} A_n(t)e^{j[w_n t+\phi_n(t)]} \tag{2.2}$$

where $w_n = w_0 + n\triangle w$. This is a continuous-time signal. The variables $A_n(t)$ and $\phi_n(t)$ on the frequency of a particular carrier are fixed values over one symbol period, thus can be rewritten as constants:

$$A_n(t) \Rightarrow A_n,\ \phi_n(t) \Rightarrow \phi_n$$

. If the signal is sampled with a sampling frequency of $1/T$, then the sampled signal can be represented by

$$S_s(kT) = \frac{1}{N}\sum_{n=0}^{N-1} A_n e^{j[(w_0+n\triangle w)kT+\phi_n]} \tag{2.3}$$

Besides, the symbol time is restricted to be longer than what the signal can be analyzed to N samples. It is convenient to sample over the period of one data symbol, thus

$$\tau = NT.$$

To simplify the signals, let $w_0 = 0$. Then the signal becomes

$$S_s(kT) = \frac{1}{N}\sum_{n=0}^{N-1} A_n e^{j[(n\triangle w)kT+\phi_n]}. \tag{2.4}$$

As we know, the form of the inverse discrete Fourier transform (IDFT) is

$$x(n) = \frac{1}{N}\sum_{k=0}^{N-1} X(w_k)e^{j\frac{2\pi kn}{N}}. \tag{2.5}$$

Since the factor $A_n e^{j\phi_n}$ is constant in the sampled frequency domain, (2.4) and (2.5) are equivalent if

$$\triangle f = \frac{\triangle w}{2\pi} = \frac{1}{NT} = \frac{1}{\tau}, \tag{2.6}$$

which is equivalent to the condition for "orthogonality" discussed before. Thus as a conclusion, using DFT to define the OFDM signal can maintain the orthogonality. Figure 2.2 displays a schematic picture of the frequency response of the individual subchannels in an OFDM symbol. In this figure, the individual subchannels of the system are separated and orthogonal from each other.

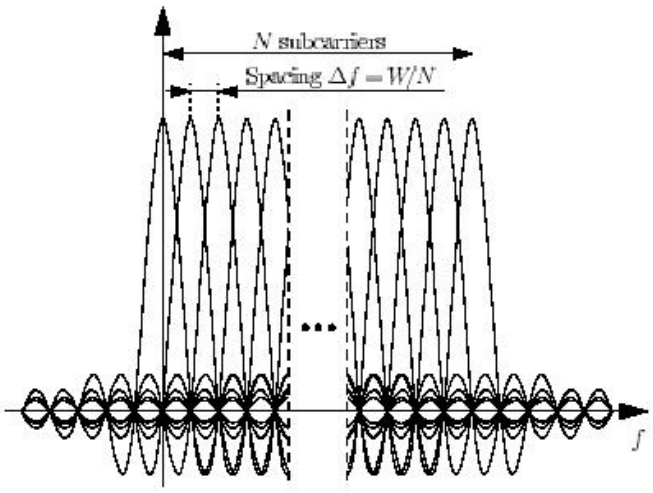

Fig. 2.2: A symbolic picture of the individual subchannels for an OFDM system with N tones over a bandwidth W (from [7]).

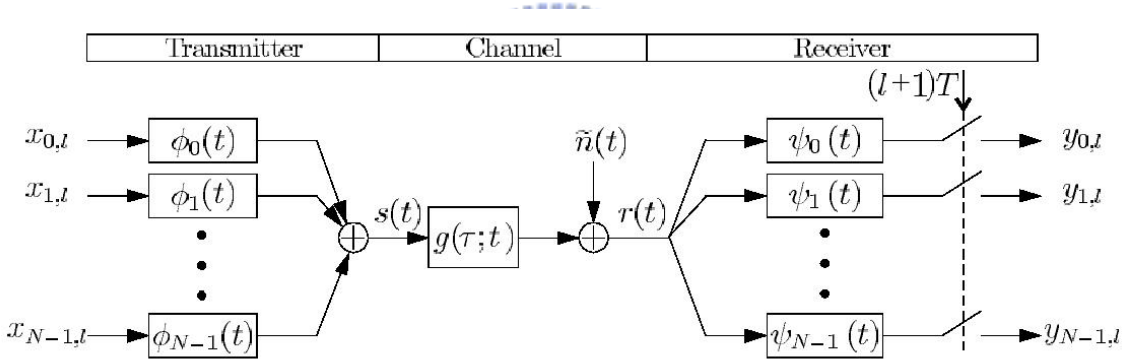

Fig. 2.3: Baseband OFDM system model (from [7]).

2.1.2 Continous-time model of OFDM including the concept of cyclic prefix

The continuous-time OFDM model presented in the Figure 2.3 can be considered as the ideal baseband OFDM system model, which in practice is digitally synthesized and will be discussed in the next section. We start to introduce the continuous model with the waveforms used in the transmitter and proceed all the way to the receiver.

- **Transmitter**

  Assumeing an OFDM system with N subcariers, a bandwidth of W Hz and aymbol

length of T seconds, of which T_g seconds is the length of the cyclic prefix, the transmitter uses the following waveforms

$$\phi_k(t) = \begin{cases} \frac{1}{\sqrt{T-T_g}} e^{j2\pi \frac{W}{N} k(t-T_g)} & \text{if } t \in [0, T], \\ 0, & \text{otherwise.} \end{cases} \tag{2.7}$$

where $T = N/W + T_g$. Note that $\phi_k(t) = \phi_k(t + N/W)$ when t is within the cyclic prefix $[0, T_g]$. Since $\phi_k(t)$ is a rectangular pulse modulated on the carrier frequency kW/N, the common interpretation of OFDM is that it uses N subcarriers, each carrying a low bit-rate. The waveforms $\phi_k(t)$ are used in the modulation and the transmitted baseband signal for OFDM symbol number l as

$$s_l(t) = \sum_{k=0}^{N-1} x_{k,l} \cdot \phi_k(t - lT), \tag{2.8}$$

where $x_{0,l}, x_{1,l}, \cdots, x_{N-1,l}$ are complex numbers from a set of signal constellation points. When an infinite sequence of OFDM symbols is transmitted, the output from the transmitter is a juxtaposition of individual OFDM symbols as

$$s(t) = \sum_{l=-\infty}^{\infty} s_l(t) = \sum_{l=-\infty}^{\infty} \sum_{k=0}^{N-1} x_{k,l} \phi_k(t - lT). \tag{2.9}$$

- **Physical channel**

  We assume that the support of the (possibly time variant) impulse response $g(\tau; t)$ of the physical channel is restricted to the interval $\tau \in [0, T_g]$, i.e., to the length of the cyclic prefix. The received signal becomes

$$r(t) = (g \times s)(t) = \int_0^{T_g} g(\tau; t) s(t - \tau) d\tau + \tilde{n}(t), \tag{2.10}$$

  where $\tilde{n}$ is additive, white, and complex Gaussian channel noise.

- **Receiver**

  The OFDM receiver consists of a filter bank, matched to the last part $[T_g, T]$ of the transmitter waveforms $\phi_k(t)$, i.e.,

$$\psi_k(t) = \begin{cases} \phi_k^*(T - t) & \text{if } t \in [0, T - T_g], \\ 0, & \text{otherwise.} \end{cases} \tag{2.11}$$

Effectively this means that the cyclic prefix is removed in the receiver. Since the cyclic prefix contains all ISI from the precious symbol, the sampled output from the receiver filter bank contains no ISI. Hence we can ignore the time index l when calculating the sampled output at the kth matched filter. By using (2.9), (2.10), and (2.11), we get

$$\begin{aligned} y_k = & \ (r \times \psi_k)(t) \mid_{t=T} \\ = & \ \int_{-\infty}^{\infty} r(t)\psi_k(T-t)dt \\ = & \ \int_{T_g}^{T}(\int_0^{T_g} g(\tau;t)[\sum_{k'=0}^{N-1} x_{k'}\phi_{k'}(t-\tau)]d\tau)\phi_k^*(t)dt \\ & + \int_{T_g}^{T} \tilde{n}(T-t)\phi_k^*(t)dt. \end{aligned} \tag{2.12}$$

We consider the channel to be fixed over the OFDM symbol interval and denote it by $g(\tau)$, which gives

$$y_k = \sum_{k'=0}^{N-1} \int_{T_g}^{T} (\int_0^{T_g} g(\tau)\phi_{k'}(t-\tau)d\tau)\phi_k^*(t)dt + \int_{T_g}^{T} \tilde{n}(T-t)\phi_k^*(t)dt. \tag{2.13}$$

The integration intervals are $T_g < t < T$ and $0 < \tau < T_g$, which implies that $0 < t-\tau < T$ and the inner integral can be written as

$$\begin{aligned} \int_0^{T_g} g(\tau)\phi_{k'}(t-\tau)d\tau = & \ \int_0^{T_g} g(\tau)\frac{e^{j2\pi k'(t-\tau-T_g)W/N}}{\sqrt{T-T_g}}d\tau \\ = & \ \frac{e^{j2\pi k'(t-T_g)W/N}}{\sqrt{T-T_g}} \int_0^{T_g} g(\tau)e^{-j2\pi k'\tau W/N}d\tau, \ \ T_g < t < T. \end{aligned} \tag{2.14}$$

The latter part of this expression is the sampled frequency response of the channel at frequency $f = k'W/N$, i.e., at the k'th subcarrier frequency:

$$h_{k'} = G(k'\frac{W}{N}) = \int_0^{T_g} g(\tau)e^{-j2\pi k'\tau W/N}d\tau, \tag{2.15}$$

where $G(f)$ is the Fourier transform of $g(\tau)$. Using this notation, the output from the receiver filter bank can be simplified to

$$\begin{aligned} y_k = & \ \sum_{k'=0}^{N-1} x_{k'} \int_{T_g}^{T} \frac{e^{j2\pi k'(t-T_g)W/N}}{\sqrt{T-T_g}} h_{k'}\phi_k^*(t)dt + \int_{T_g}^{T} \tilde{n}(T-t)\phi_k^*(t)dt \\ = & \ \sum_{k'=0}^{N-1} x_{k'}h_{k'} \int_{T_g}^{T} \phi_{k'}(t)\phi_k^*(t)dt + n_k, \end{aligned} \tag{2.16}$$

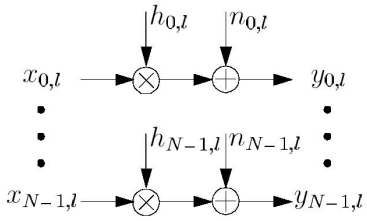

Fig. 2.4: The continuous-time OFDM system interpreted as parallel Gaussian channels.

where $n_k = \int_{T_g}^{T} \tilde{n}(T-t)\phi_k^*(t)dt$. Since the transmitter filters $\phi_k(t)$ are orthogonal, the following equation is thus obtained.

$$\int_{T_g}^{T} \phi_{k'}(t)\phi_k^*(t)dt = \int_{T_g}^{T} \frac{e^{j2\pi k'(t-T_g)W/N}}{\sqrt{T-T_g}} \frac{e^{-j2\pi k(t-T_g)W/N}}{\sqrt{T-T_g}} dt = \delta[k-k']. \quad (2.17)$$

According to (2.16), we know that

$$y_k = h_k x_k + n_k, \quad (2.18)$$

The benefit of a cyclic prefix is twofold: it avoids both ISI (since it acts as a guard space) and ICI (since it maintains the orthogonality of the subcarriers). By re-introducing the time index l, we may now view the OFDM system as a set of parallel Gaussian channels, according to Figure 2.4.

2.1.3 Discrete-time model

An entirely discrete-time model of and OFDM systme is displayed in Figure 2.5. Compared to the continous-time model, the modulation and demodulation are replaced by an inverse DFT (IDFT) and a DFT respectively and the channel is a discrete-time convolution. The cyclic prefix operates in the same fashion in this system and the calculations can be performed in essentially the same way. The main difference is that all integrals are replaced by sums.

As far as the receiver is concerned, the use of a cyclic prefix longer than the channel response will transform the linear convolution in the channel into a cyclic convolution.

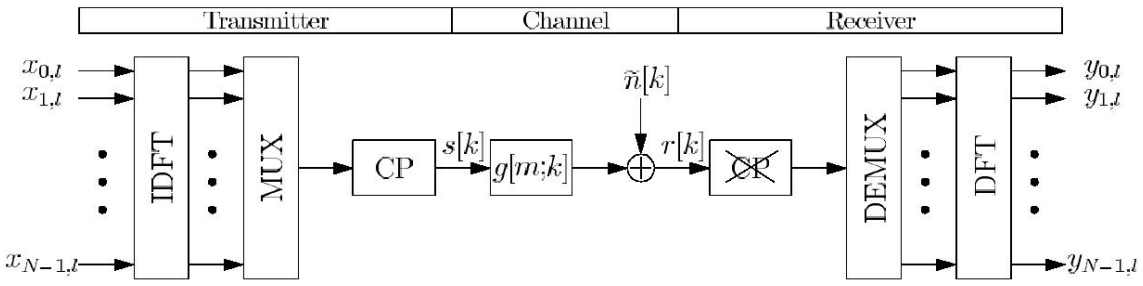

Fig. 2.5: Discrete-time OFDM system (from [7]).

Denoting cyclic convolution by "$\otimes$", we can write the whole OFDM system as

$$\begin{aligned} y_l &= DFT(IDFT(\mathbf{x_l}) \otimes \mathbf{g_l} + \tilde{\mathbf{n}}) \\ &= DFT(IDFT(\mathbf{x_l}) \otimes \mathbf{g_l}) + \mathbf{n_l}, \end{aligned} \tag{2.19}$$

where $\mathbf{y_l}$ contains the N received data points, $\mathbf{x_l}$ is the N transmitted constellation points, $\mathbf{g}$ is the channel impulse response of the channel (padded with zeros to obtain a length of N), and $\tilde{\mathbf{n}}$ is the channel noise. Since the channel noise is assumed to be white Gaussian, the term $\mathbf{n_l} = DFT(\tilde{\mathbf{n}}_\mathbf{l})$ represents uncorrelated Gaussian noise. Furthermore, we use the fact that the DFT of two cyclically convolved signals is equivalent to the product of their individual DFTs. Denoting element-by-element multiplication by "$\cdot$" , the above expression can thus be written as

$$\mathbf{y_l} = \mathbf{x_l} \cdot DFT(\mathbf{g_l}) + \mathbf{n_l} = \mathbf{x_l} \cdot \mathbf{h_l} + \mathbf{n_l}, \tag{2.20}$$

where $\mathbf{h_l} = DFT(\mathbf{g_l})$ is the frequency response of the channel. Therefore we have obtained the same type of parallel Gaussian channels as the continuous-time model. The only difference is that the channel attenuations $\mathbf{h_l}$ are given by the N-point DFT of the discrete-time channel, instead of the sampled frequency response as in (2.15).

2.1.4 Imperfections of OFDM

Depending on the mathematical analyzed situation disscused before, imperfections in a real OFDM system may be ignored or explicitly included in the model. Below we mention of the imperfections and their corresponding effects.

- **Dispersion**

  Both time and frequency dispersion of the channel can destroy the orthogonality of the system, i.e., introduce both ISI and ICI. If these effects are not sufficiently mitigated by e.g., a cyclic prefix and a large inter-carrier spacing, they have to be included in the model. One way of modelling these effects is an increase of the additive noise.

- **Nonlinearities and clipping distortion**

  OFDM systems have high peak-to-average power ratios and high demands on linear amplifiers. Nonlinearities in amplifiers may cause both ISI and ICI in the system. Especially, if the amplifiers are not designed with proper output back-off (OBO), the clipping distortion may cause severe degradation.

- **External interference**

  In wireless systems, the external interference usually stems from radio transmitters and other types of electronic equipment in the vinciniy of the receiver.

2.2 OFDMA

The basic idea of OFDMA is OFDM based frequency division multiaccess. In OFDM, a channel is divided into carriers which are used only by one user. In OFDMA, the carriers are divided into subchannels. Each subchannel is also divided into subcarriers that form one unit in frequency allocation. A subchannel may be intended for more than one receiver (user) in the downlink. Likewise, a transmitter (user) may be assigned one or more subchannels in the uplink, and several transmitters can transmit in parallel. Thus the bandwidth can be assigned dynamically to the users according to their needs.

In order to support multiple users, the control mechanism becomes more complex. Besides, the OFDMA system has more implementation issues. For example, the power control may be needed for the uplink to make signals from different users have equal

power at the receiver, and all users have to adjust their transmitting times to make them aligned. Some issues in the context of IEEE 802.16a will be discussed in the next chapter.

Chapter 3

Introduction to IEEE 802.16a [4]

3.1 Background of 802.16a

The following three paragraphs are largely taken from [9].

Broadband wireless access (BWA) is a way to meet escalating business demand for rapid internet connection and integrated data, voice and video services. BWA can extend fiber optic networks and provide more capacity than cable networks or digital subscriber lines (DSL). One of the most compelling aspects of BWA technology is that networks can be created in just weeks by deploying a small number of base stations on buildings or poles to create high-capacity wireless access systems. BWA has had limited reach so far, in part because there was not a universal standard. While providing such a standard is important for developed countries, it is even more important for the developing world where wired infrastructures are limited.

The Institute of Electrical and Electronics Engineers Standards Association (IEEE-SA) sought to make BWA more widely available by developing IEEE Standard 802.16. The 802.16 standard defines the Wireless MAN (metropolitan area network) air interface specification (officially known as the IEEE WirelessMAN standard). This wireless broadband access standard could supply the missing link for the “last mile” connection in wireless metropolitan area networks [10]. It focuses on the efficient use of bandwidth between 10 and 66 GHz and defines a medium access control (MAC) layer that supports multiple physical layer specifications customized for the frequency band of use.

IEEE 802.16's Task Group developed IEEE Standard 802.16a, an amendment to IEEE Standard 802.16. The amendment covers "Medium Access Control Modifications and Additional Physical Layer Specifications for 2-11 GHz." Both licensed and license-exempt bands are included [11]. This standard was published in April 2003. It specifies the air interface of fixed (stationary) broadband wireless access systems providing multiple services. The medium access control layer is capable of supporting multiple physical layer specifications optimized for the frequency bands of application.

There are several system mode in 802.16a: SC (single carrier), OFDM, and OFDMA. We consider the OFDMA option in our research. Before a more detailed technical overview of the IEEE 802.16a standard, we introduce some frequently used terms below [4].

- **SS:** *subscriber station.* It is usually known as the mobile station or the user.
- **BS:** *base station.* It is a generalized equipment set providing connectivity, management, and control of the subscriber station.
- **DL:** *down-link.* The direction of transmission from the BS to the SS.
- **UL:** *up-link.* The direction of transmission from the SS to the BS, which is opposite to DL.
- **MAC:** *medium access control layer.* It is used to control the system access and provide the link of data from the upper layer to the lower layer (i.e., the PHY layer). The system access functions include bandwidth allocation, connection establishment, connection maintenance, and security.
- **PHY:** *physical layer.* It handles the data trnsmission and may include use of multiple transmission technologies, each appropriate to a particular frequency range and application.
- **TDD:** *time division duplex.* A duplex scheme where uplink and downlink transmissions occur at different times but may share the same frequency.

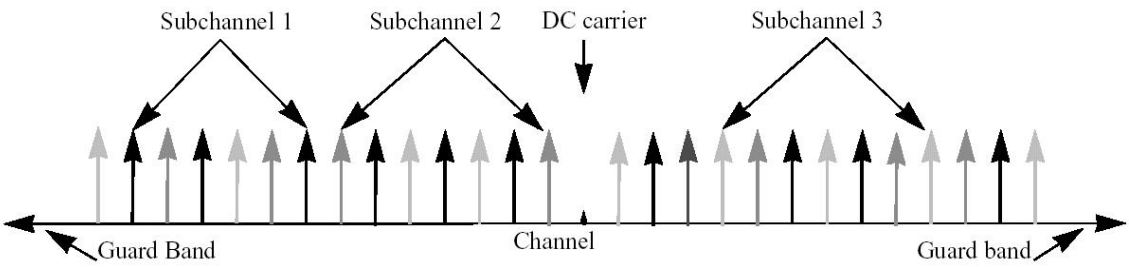

Fig. 3.1: OFDMA frequency symbol description (example for 3 subchannels) (from [4]).

- **CP:** *cyclic prefix*. A cyclic prefix is a copy of the last part of the OFDM symbol which is prepended to the transmitted symbol.

We stress more on the DL of PHY layer in the below subsections.

3.2 Generic OFDMA Symbol Description

3.2.1 Frequency domain description

An OFDMA symbol in frequency domain is made up from several carrier types:

- Data carriers — for data transmission.
- Pilot carriers — for various estimation purposes.
- Null carriers — no transmission at all, for guard bands and DC carrier. (The purpose of the guard bands is to enable the signal to naturally decay and create the FFT "brick wall" shaping.)

The allocations of the three kinds of carriers will be given later.

In the OFDMA mode, active carriers are devided into subsets of carriers, each subset is termed a subchannel. In the DL, a subchannel may be intended for different groups of receivers; similarly, a transmitter may be assigned on or more subchannels in the UL, serveral transmitters may transmit in parallel. The concept is shown in Fig. 3.1.

3.2.2 Time domain description

Inverse-Fourier-transforming from frequency domain OFMDA symbol creates the time domain waveform; this time duration is referred to as the useful symbol time T_g. A copy of the last T_g μs of the useful symbol period is termed cyclic prefix,as we introuduced in section 2.1. It is used to collect multipath while maintaining the orthogonality of the tones. The transmitter energy increases with the length of the guard time while the receiver energy remains the same, so the loss in SNR (in dB) can be calculated as,

$$10log_{10}(1 - \frac{T_g}{T_b + T_g}) = 10log_{10}(\frac{T_b}{T_b + T_g}), \tag{3.1}$$

where the defination of T_b and T_g are the same as in chapter 2. Using a cyclic extension, the samples required for performing the FFT at the receiver can be taken anywhere over the length of the extended symbol. This provides multipath immunity as well as a tolerance for symbol time synchronization errors.

3.3 OFDMA Symbol Parameters and Transmitted Signal

3.3.1 Primitive parameters

Four primitive parameters characterize the OFDMA symbol:

- BW. This is the nominal channel bandwidth. And it equals 10 MHz in our system simulation.
- (F_s/BW). This is the ratio of "sampling frequency" to the nominal channel bandwidth. This value is set to $8/7$.
- (T_g/T_b). This is the ratio of CP time to "useful" time. We use $1/8$ in our system.
- N_{FFT}. This is the number of points in the FFT. The OFDMA PHY defines this value to be equal to 2048.

3.3.2 Derived parameters

The following parameters are defined in terms of the primitive parameters.

- $F_s = (F_s/BW) \cdot BW$ = sampling frequency. The value equals $10 \times 8/7 = 11.42$ MHz.
- $\triangle f = F_s/N_{FFT}$ = carrier spaing =5.57617 KHz.
- $T_b = 1/\triangle f$ = useful time =179.33 μs.
- $T_g = (T_g/T_b) \cdot T_b$ = CP time =22.4 μs.
- $T_s = T_b + T_g$ = OFDM symbol time =201.9 μs.
- $1/F_s$= sample time =87.5657 ns.

3.3.3 Transmitted signal

Eq. (3.2) specifies the transmitted signal voltage to the antenna, as a function of time, during any OFDMA symbol.

$$S(t) = Re\{e^{j2\pi f_c t} \sum_{\substack{k=-N_{used}/2 \\ k\neq 0}}^{N_{used}/2} a_k \cdot e^{j2\pi k \triangle f (t-T_g)}\} \tag{3.2}$$

where:

- t = time, elapsed since the beginning of the subject OFDM symbol, with $0 < t < T_s$.
- a_k= a complex number; the data to be transmitted on the carrier whose frequency offset index is k, during the subject OFDM symbol. It specifies a point in a QAM constellation.
- T_g= guard time.
- T_s= OFDM symbol duration, including guard time.
- $\triangle f$= carrier frequency spacing.

3.4 OFDMA Carrier Allocation

We will compare the different carrier allocations between DL and UL, but this thesis is focused on the DL carrier allocation.

For OFDMA, $F_s = BW \cdot 8/7$. Subtracting the DC carrier and the guard tones from N_{FFT}, one obtains the set of used carriers N_{used}. The carriers are allocated to pilot carriers and data carriers in both DL and UL. But the difference beween DL and UL is that, in the downlink, the pilot tones are allocated first. The remainder of carriers are subchannels which are used exclusively for data. On the other hand in the UL, the set of used carriers is first partitioned into subchannels, and then the pilot carriers are allocated from within each subchannel. Thus, in the DL, there is one set of common pilot carriers, but in the UL, each subchannel contains its own set of pilot carriers.

In the sequel, carriers are identified by a carrier index. The frequency offset index of a particular carrier is specified terms of its carrier index as

$$k_{foi} = \begin{cases} k_{ci} - N_{used}/2, & k_{ci} < N_{used}/2, \\ k_{ci} - N_{used}/2 + 1, & k_{ci} \geq N_{used}/2, \end{cases} \tag{3.3}$$

where:

- k_{foi} = frequency offset index,
- k_{ci} = carrier index, and
- N_{used} = number of used carriers.

3.4.1 DL assignment of pilots

The N_{used} used carriers are partitioned into fixed-location pilots, variable location pilots, and data subchannels. The carrier indices of the fixed-location pilots never change. These indices are the members of the set BasicFixedLocationPilots, and will be listed later. The variable-location pilots shift their location every symbol repeating every 4 symbols,

according to the following formula:

$$varLocPilot_k = 3L + 12P_k \tag{3.4}$$

where:

- $varLocPilot_k$ = carrier index of a variable-location pilot,
- $L \in 0 \cdots 3$ is a function of the symbol index, modulo 4,
- $P_k \in \{0, 1, 2, \cdots, N_{varLocPilots} - 1\}$.

Notice that, L does not simply increment from one symbol to the next, but follows the sequence L=0, 2, 1, 3, 0, 2,$\cdots$.

In some cases, a variable-location pilot will coincide with a fixed-location pilot. The sets of BasicFixedLocationPilots are designed so that the number of coinciding pilots is the same for every L, i.e. 8. The allocation of pilot carriers is illustrated in Figure 3.2.

3.4.2 Partitioning of data carriers into subchannels

After mapping the pilots, the remainder of the used carriers are the data subchannels. Since the variable location pilots change location in each symbol, repeating every fourth symbol, the locations of the carriers in the data subchannels also need to change.

The remaining carriers are partitioned into groups of contiguous carriers. Each subchannel consists of one carrier from each of these groups. The number of groups is therefore equal to the number of carriers per subchannel, which is denoted $N_{subcarriers}$. Likewise, the number of carriers in a group is equal to the number of subchannels, and it is denoted $N_{subchannels}$. Thus the number of data carriers is equal to $N_{subcarriers} \times N_{subchannels}$.

The exact subchannels partition is given by

$$\begin{aligned} carrier(n, s) = \; & N_{subchannels} \cdot n + \{p_s[n_{mod(N_{subchannels})}] \\ & + ID_{cell} \cdot ceil[(n+1)/N_{subchannels}]\}_{mod(N_{subchannels})} \end{aligned} \tag{3.5}$$

where:

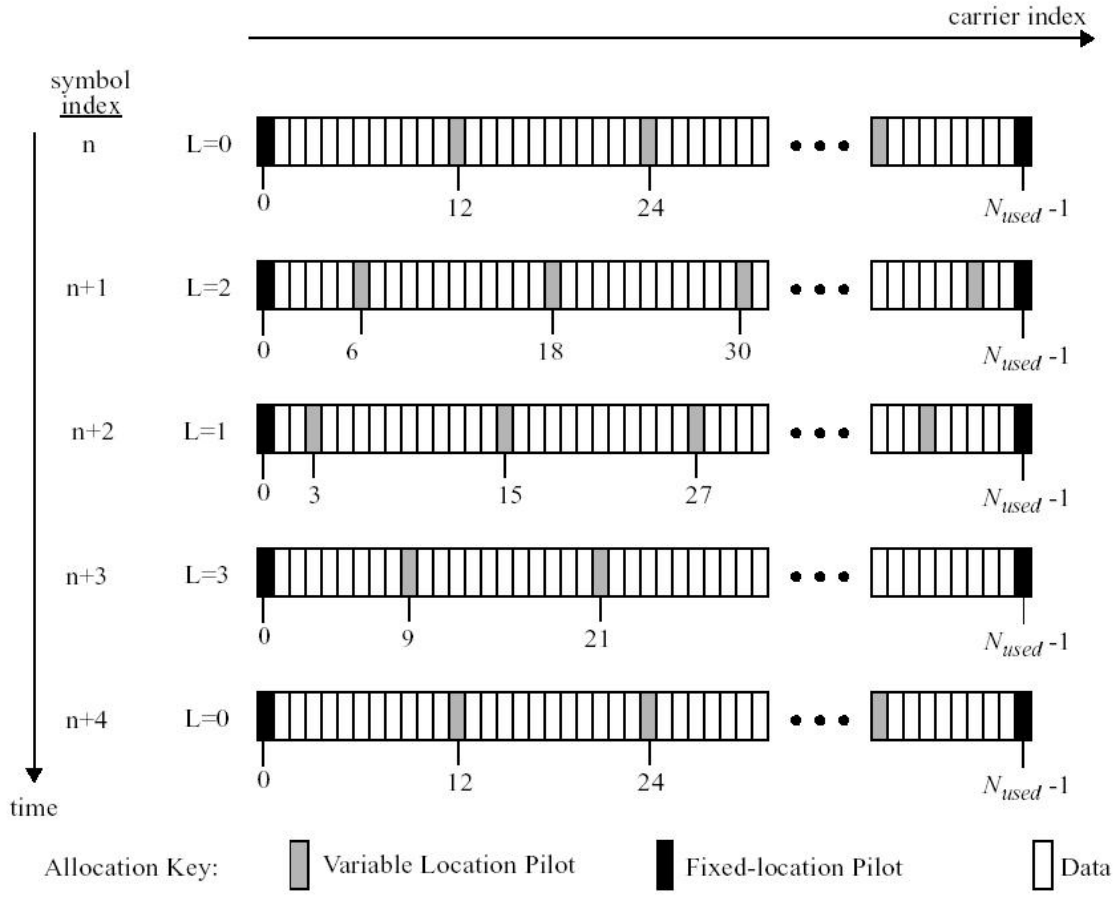

Fig. 3.2: Carrier allocation in 802.16a OFDMA DL (from [4]).

- $carrier(n, s)$ =carrier index of carrier n in subchannel s.
- s = index number of a subchannel, from the set [0, $\cdots$, $N_{subchannels} - 1$].
- n = carrier-in-subchannel index from the set [0, $\cdots$, $N_{subcarriers} - 1$].
- $N_{subchannels}$ = number of subchannels.
- $p_s[j]$ = the series obtained by rotating $\{PermutationBase_0\}$ which is given in the table 3.1 cyclically to the left s times.
- $ceil[\,]$ = ceiling function which rounds its argument up to the next integer.
- ID_{cell} = a postive integer assigned by the MAC to identify this particular base-

Table 3.1: OFDMA DL Carrier Allocation

Parameter	**Value**
Number of DC carriers	1
Number of guard carriers, left	173
Number of guard carriers, right	172
N_{used}, number of used carriers	1702
Total number of carriers	2048
$N_{varLocPilots}$	142
Number of fixed-location pilots	32
Number of variable-location pilots which coincide with fixed-location pilots	8
Total number of pilots	166
Number of data carriers	1536
$N_{subchannels}$	32
$N_{subcarriers}$ per subchannel	48
Number of data carriers per subchannel	48
BasicFixedLocationPilots	{0, 39, 261, 330, 342, 351, 522, 636, 645, 651, 708, 726, 756, 792, 849, 855, 918, 1017, 1143, 1155, 1158, 1185, 1206, 1260, 1407, 1419, 1428, 1461, 1530, 1545, 1572, 1701}
$\{PermutationBase_0\}$	{3, 18, 2, 8, 16, 10, 11, 15, 26, 22, 6, 9, 27, 20, 25, 1, 29, 7, 21, 5, 28, 31, 23, 17, 4, 24, 0, 13, 12, 19, 14, 30 }

station cell.

- $X_{mod(k)}$ = the remainder of the quotient X/k, which is at most $k-1$.

The numerical parameters are given in Table 3.1.

3.5 Modulation

3.5.1 Data modulation

There are three types of modulations, namely, QPSK, 16QAM and 64 QAM, in IEEE 802.16a OFDMA mode. Gray-mapped QPSK and 16QAM as shown in Figure 3.3 shall be supported, whereas the support of 64QAM is optional. The constellations of the three kinds of modulations shall be normalized by multiplying the constellation point with the

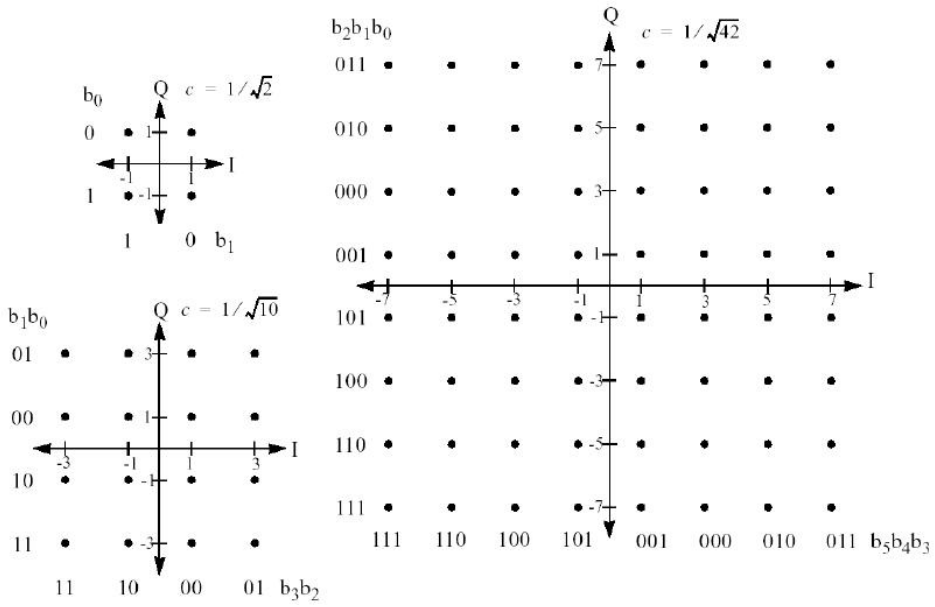

Fig. 3.3: QPSK, 16QAM and 64 QAM constellations (from [4]).

indicated factor c to achieve equal average power.

3.5.2 Pilot modulation

Pilot carriers shall be inserted into each data burst in order to constitute the symbol, and they shall be modulated according to their carrier location within the OFDMA symbol. The PRBS which denotes pseudo random binary sequence w_k should be generated as shown in Fig. 3.4. The polynomial for the PRBS generator is $X^{11} + X^9 + 1$.

When using data transmission on the DL, the initialization vector of the PRBS is [11111111111] except for the OFDMA DL PHY preamble, which is [01010101010]. These initializations result in the sequence w_k = 11111111110000000001$\cdots$ in the DL data signal. The PRBS shall be initialized so that its first output bit coincides with the first usable carrier. A new value shall be generated by the PRBS on every usable carrier. The pilot cariers shall be modulated according to the following formula:

$$\Re\{C_k\} = \frac{8}{3}(\frac{1}{2} - w_k), \Im\{C_k\} = 0. \tag{3.6}$$

We now turn to the downlink channel estimation in the next chapter.

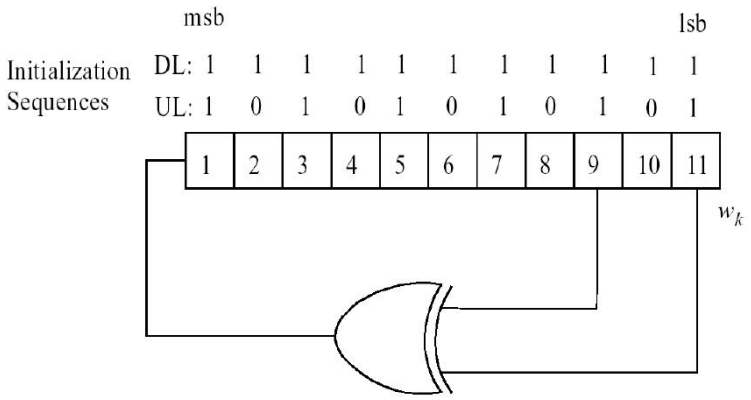

Fig. 3.4: PRBS generator for pilot modulation.

Chapter 4

Downlink Channel Estimation

There are three main subjects in this chapter, which are channel estimation on pilot subcarriers, interploation schemes and time domain improvement methods.

We use the LS technique to estimate the channel response on pilots. Three kinds of interpolation schemes are used, including of linear, second order and cubic spline interpolations. And the four kinds of time domain improvement methods are moving average, exponential average, LMS adaption and 2-Dimensional interpolation. All the techniques are discussed individually in the following sections.

4.1 Channel Estimation on Pilot Subcarriers

4.1.1 Pilot information

Channel estimators usually need some kind of pilot information as a point of reference. A fading channel requires constant tracking, so pilot information has to be transmitted more or less continuously. Decision-directed channel estimation can also be used, but even in these types of schemes, pilot information has to be transmitted regularly to mitigate error propagation [7].

In general, the fading channel can be viewed as a two-dimensional (2-D) signal (time and frequency), which is sampled at pilot positions and the channel attenuations between pilots are estimated by interpolation.

4.1.2 LS and MMSE estimations

Based on a priori known data, we can estimate the channel information on pilot carriers roughly by the least-square (LS) or the minimun mean square error (MMSE) estimator. An LS estimator minimizes the following squared error [12]:

$$||\mathbf{Y} - \hat{\mathbf{H}}_{LS}\mathbf{X}||^2 \tag{4.1}$$

where $\mathbf{Y}$ is the received data and $\mathbf{X}$ is priori known pilots, and both are N×1 vectors where N is the OFDM FFT size. $\hat{\mathbf{H}}_{LS}$ is a N×N matrix whose values are 0 except at pilot locations m_i where $i = 0, \cdots, N_p - 1$.

$$\hat{\mathbf{H}}_{LS} = \begin{bmatrix} H_{m_0,m_0} & \cdots & 0 & \cdots & 0 & \cdots & 0 \\ 0 & \cdots & H_{m_1,m_1} & \cdots & 0 & \cdots & 0 \\ 0 & \cdots & 0 & \cdots & H_{m_2,m_2} & \cdots & 0 \\ 0 & \cdots & 0 & \cdots & 0 & \cdots & 0 \\ 0 & \cdots & 0 & \cdots & 0 & \cdots & H_{m_{N_p-1},H_{m_{N_p-1}}} \end{bmatrix}. \tag{4.2}$$

Therefore the (4.1) can be rewritten as

$$[Y(m) - \hat{H}_{LS}(m)X(m)]^2, \text{ for all } m = m_i. \tag{4.3}$$

Then the estimate of pilot signals, based on one observed OFDM symbol, is given by

$$\hat{H}_{LS}(m) = \frac{Y(m)}{X(m)} = \frac{X(m)H(m) + N(m)}{X(m)} = H(m) + \frac{N(m)}{X(m)} \tag{4.4}$$

where $N(m)$ is the complex white Gaussian noise on subcarrier m. We collect $H_{LS}(m)$ into $\hat{\mathbf{H}}_{\mathbf{p,LS}}$, an $N_p \times 1$ vector where N_p is the total pilot numbers as

$$\begin{aligned} \hat{\mathbf{H}}_{p,LS} = & \ [H_{p,LS}(0)\ H_{p,LS}(1)\ \cdots H_{p,LS}(N_p-1)]^T \\ = & \ \mathbf{X}_p^{-1}\mathbf{Y}_p \\ = & \ [\tfrac{Y_p(0)}{X_p(0)}, \tfrac{Y_p(1)}{X_p(1)}, \ldots, \tfrac{Y_p(N_p-1)}{X_p(N_p-1)}]^T, \end{aligned} \tag{4.5}$$

where $\mathbf{X}_p$ and $\mathbf{Y}_p$ are the collections of the transmitted and the received data on the pilot subcarriers individually. The LS estimate of $\mathbf{H}_p$ based on one OFDM symbol only is susceptible to Gaussian noise, thus an estimator better than the LS estimator is preferable.

The minimum mean-square error (MMSE) estimate has been shown to be better than the LS estimate for channel estimation in OFDM systems. But the major drawback of the MMSE estimate is its high complexity, which grows exponentially with the observation samples [13]. A low-rank approximation is applied in a linear minimum mean squared error (LMMSE) estimator that uses the frequency correlation of the channel. The mathematical representation for the LMMSE estimator [13] of pilot signals is

$$\begin{aligned}\hat{\mathbf{H}}_{p,lmmse} &= \mathbf{R}_{H_pH_{p,LS}}\mathbf{R}^{-1}_{H_{p,LS}H_{p,LS}}\hat{\mathbf{H}}_{p,LS} \\ &= \mathbf{R}_{H_pH_p}(\mathbf{R}_{H_pH_p}+\sigma_n^2(\mathbf{X}_p\mathbf{X}_p^H)^{-1})^{-1}\hat{\mathbf{H}}_{p,LS} \qquad (4.6)\end{aligned}$$

where $\hat{\mathbf{H}}_{p,LS}$ is the least-square estimate of $\mathbf{H}_p$ in (4.5), σ_n^2 is the variance of the Gaussian white noise, and the covariance matrices are defined by

$$\mathbf{R}_{H_pH_{p,LS}} = E\{\mathbf{H}_p\mathbf{H}^H_{p,LS}\}, \qquad (4.7)$$

$$\mathbf{R}_{H_{p,LS}H_{p,LS}} = E\{\mathbf{H}_{p,LS}\mathbf{H}^H_{p,LS}\}, \qquad (4.8)$$

$$\mathbf{R}_{H_pH_p} = E\{\mathbf{H}_p\mathbf{H}^H_p\}. \qquad (4.9)$$

Note that there is a matrix inverse involved in the MMSE estimator, which must be calculated every time, and the computational complexity of matrix inversion requires $O(N_p^3)$ arithmetic operations [14]. We also need to use the statistical properties of the unknown channel. Therefore, we use the LS estimator which requires only $O(N_p)$ operations instead of the LMMSE one due to the concerns of complexity and the unknown information.

4.2 Interpolation Schemes

After knowing the channel response on the pilot carriers, we need to use interpolation to get the response on the rest of the carriers. Three interpolation methods are introduced here, and the performance comparison will be discussed in the next chapter.

4.2.1 Linear interpolation

Linear interpolation is a commonly used method of interpolations. It does the interpolation simply with two known data adjacent to the unknown ones. The following is the mathematical expression [1]:

$$H_e(k) = H_e(m+l) = (H_p(m+1) - H_p(m))\frac{l}{L} + H_p(m) \tag{4.10}$$

where $\{H_p(k), k = 0, 1, \cdots, N_p\}$ is the channel frequency response at pilot subcarriers, L is the distance between the two given data, that is, the pilot sub-carriers spacing, and $0 \leq l < L$.

4.2.2 Second order interpolation

Theoretically, using higher-order polynomial interpolation will fit the channel response better than the linear interpolation [15]. However, the computational complexity grows as the order is increased. Here we consider the second order polynomial interpolation,and it is also called Gaussian second order estimation. It is given as a solution to the second order polynomial with respect to l/L by using three reference signals. The interpolation is obtained using three successive pilot subcarriers signal as follows [16]:

$$\begin{aligned} H_e(k) &= H_e(m+l) \\ &= c_1 H_p(m-1) + c_0 H_p(m) + c_{-1} H_p(m+1) \end{aligned} \tag{4.11}$$

where

$$\begin{cases} c_1 = \frac{\alpha(\alpha-1)}{2}, \\ c_0 = -(\alpha-1)(\alpha+1), \\ c_{-1} = \frac{\alpha(\alpha+1)}{2}, \\ \alpha = \frac{l}{L}. \end{cases}$$

The notations are the same as they are in linear interpolation.

4.2.3 Cubic spline interpolation [17], [18]

Cubic Spline is one very effective, well-behaved, computationally efficient interpolation. The approach is to fit cubic polynomials to adjacent pairs of points and choose the values of the two remaining parameters associated with each polynomials such that the polynomails covering adjacent intervals agree with one another in both slope and curvature at their common endpoint. The piecewise-cubic interpolating function $g(x)$ that results is twice continuously differentiable over $[x_0, x_N]$. And the cubic spline interpolation is developed by the following algorithm.

Development of the cubic spline algorithm

The goal is to construct a piecewise-cubic polynomial $g(x)$ that interpolates the real-valued function $f(x)$ at the $N+1$ points $x_0 < x_1 < \cdots < x_N$ at which the values of $f(x)$ are known. So, we construct $g(x)$ on each interval $[x_i, x_{i+1}]$, $i = 0, 1, \cdots, N-1$, is a cubic polynomial

$$P_i(x) = c_{0,i} + c_{1,i}(x - x_i) + c_{2,i}(x - x_i)^2 + c_{3,i}(x - x_i)^3. \tag{4.12}$$

Once we find the coefficients $c_{j,i}$, $j = 0, \cdots, 3$; $i = 0, \cdots, N-1$, we can evaluate $g(x)$ for any point x in $[x_0, x_N]$. And the boundary condition gives us the following two equations:

$$P_i(x_i) = f(x_i), \tag{4.13}$$

$$P_i(x_{i+1}) = f(x_{i+1}). \tag{4.14}$$

Eq. (4.14) implies that $P_{i-1}(x_i) = f(x_i), \quad i = 1, \cdots, N$, which in turn guarantees $g(x)$ to be continuous on $[x_0, \cdots, x_N]$.

As we mentioned before, each $P_i(x)$ is required to interpolate at only two points. But since a cubic polynomial can interpolate a function at four points, we have freedom remaining in choosing the $P_i(x)$.

We choose our two remaining constraints as that $P_i(x_i)$ must agree with $P_{i-1}(x_i)$ in both slope and curvature; that is, we want

$$P_i'(x_i) = P_{i-1}'(x_i) \tag{4.15}$$

and

$$P_i''(x_i) = P_{i-1}''(x_i) \tag{4.16}$$

for $i = 1, \cdots, N-1$.

We let the curvatures κ_i at x_i and κ_{i+1} at x_{i+1} be parameters of $P_i(x)$. Since $P_i(x)$ is a cubic polynomial, $P_i''(x)$ is a linear polynomial constrained such that $P_i''(x_i) = \kappa_i$ and $P_i''(x_{i+1}) = \kappa_{i+1}, i = 0, 1, \cdots, N-1$. That is

$$P_i''(x) = \kappa_i \frac{x_{i+1} - x}{x_{i+1} - x_i} + \kappa_{i+1} \frac{x - x_i}{x_{i+1} - x_i} \tag{4.17}$$

Intergrating (4.17), we get

$$P_i'(x) = -\frac{\kappa_i}{2} \frac{(x_{i+1} - x)^2}{x_{i+1} - x_i} + \frac{\kappa_{i+1}}{2} \frac{(x - x_i)^2}{x_{i+1} - x_i} + \alpha_i. \tag{4.18}$$

Intergrating (4.18) gives

$$P_i(x) = -\frac{\kappa_i}{6} \frac{(x_{i+1} - x)^3}{x_{i+1} - x_i} + \frac{\kappa_{i+1}}{6} \frac{(x - x_i)^3}{x_{i+1} - x_i} + \alpha_i x + \beta_i. \tag{4.19}$$

The equation is equivalent to

$$P_i(x) = -\frac{\kappa_i}{6} \frac{(x_{i+1} - x)^3}{x_{i+1} - x_i} + \frac{\kappa_{i+1}}{6} \frac{(x - x_i)^3}{x_{i+1} - x_i} + A_i(x_{i+1} - x) + B_i(x - x_i), \quad i = 0, \cdots, N-1. \tag{4.20}$$

where A_i and B_i are constants of integration.

Applying the constraint given by (4.13), we get from (4.20) that

$$\begin{aligned} P_i(x_i) &= f(x_i) \\ &= \tfrac{\kappa_i}{6}(x_{i+1} - x_i)^2 + A_i(x_{i+1} - x_i) \end{aligned} \tag{4.21}$$

or

$$A_i = \frac{f(x_i)}{x_{i+1} - x_i} - \frac{\kappa_i}{6}(x_{i+1} - x_i), \quad i = 0, \cdots, N-1. \tag{4.22}$$

Similarly, by applying the constraint given by (4.14), we get from (4.20) that

$$\begin{aligned} P_i(x_{i+1}) = &\quad f(x_{i+1}) \\ = &\quad \tfrac{\kappa_{i+1}}{6}(x_{i+1}-x_i)^2 + B_i(x_{i+1}-x_i) \end{aligned} \tag{4.23}$$

or

$$b_i = \frac{f(x_{i+1})}{x_{i+1}-x_i} - \frac{\kappa_{i+1}}{6}(x_{i+1}-x_i), \quad i = 0, \cdots, N-1. \tag{4.24}$$

The final constraint to be satisfied is that the first derivative must be continuous. According to (4.15), (4.18) becomes

$$\begin{aligned} P_i'(x) = &\quad -\tfrac{\kappa_i}{2}\tfrac{(x_{i+1}-x)^2}{x_{i+1}-x_i} + \tfrac{\kappa_{i+1}}{2}\tfrac{(x-x_i)^2}{x_{i+1}-x_i} \\ + &\quad \tfrac{f(x_{i+1})-f(x_i)}{x_{i+1}-x_i} - \tfrac{\kappa_{i+1}-\kappa_i}{6}(x_{i+1}-x_i). \end{aligned} \tag{4.25}$$

Again, using (4.15) we can obtain

$$\begin{aligned} \kappa_{i-1}(x_i - x_{i-1}) + &\quad 2\kappa_i(x_{i+1}-x_{i-1}) + \kappa_{i+1}(x_{i+1}-x_i) \\ = &\quad 6[\tfrac{f(x_{i+1})-f(x_i)}{x_{i+1}-x_i} - \tfrac{f(x_i)-f(x_{i-1})}{x_i-x_{i-1}}], \end{aligned} \tag{4.26}$$

for $i = 1, 2, \cdots, N-1$. Once (4.26) is solved for all the κ_i, we have everything we need to find the coefficients $c_{i,j}$ of the $P_i(x)$, which in turn can get the interpolator $g(x)$.

Eq. (4.26) is a system of $N-1$ linear equation in $N+1$ unknowns κ_i, $i = 0, 1, \cdots, N$. Thus we have to determine κ_0 and κ_N to solve all the κ_i. In this work, the two values κ_0 and κ_N are set to be 0. This is equivalent to assuming that $P_0(x)$ and $P_{N-1}(x)$ approach linearity at their outer extremities.

4.2.4 Comparison and illustration of the three interpolations

The complexity of the three interpolations is compared in Table 4.1.

Fig. 4.1 shows some results obtained by interpolation using the three different interpolation schemes. The channel frequency response in static case in our simulation which will be introduced in chapter 5 is partly chosen to be the original data in the figure. And the sampled data positions is the corresponding pilot carriers. We can see from the figure, for the pilot ratio is obviously insufficient that the performances are not very good in each kind of interpolations. Thus we need to use the information of other symbols to achieve better estimation.

Table 4.1: Comparison of Computation Complexities of Several Channel Interpolation Techniques

Interpolation Technique	Computation Complexity for Each Carrier
Linear Interpolation	4MPYs + 4Adds
Second Order Interpolation	6MPYs +4Adds
Cubic Spline	At least 6MPYs + 6Adds

4.3 Time Domain Improvement Methods

After doing the interpolation, we obtained the overall estimated channel response in frequency domain. And the simulations of our channel estimation are based on static and mobile Rayleigh fading channel. Both have correlation between channel frequency responses of diffrent symbols, thus we develop a few methods to use the data of different symbols to improve our estimation. But the estimated channel is still given in frequency domain.

4.3.1 Moving average

Assuming the receiver which is the SS, has a velocity of 100 km/hr, or equivalently, 27.78 m/s. The Doppler frequency with a center frequency is 2 GHz can be calculated according to [19]

$$f_d = \frac{v}{c} \cdot f_c \cdot \cos\theta \tag{4.27}$$

where f_d is the Doppler frequency, v is the velocity of the receiver, c is the velocity of light, f_c is the center radio frequency and θ is the angle between the v and line of sight of transmitter and receiver. We thus obtain f_d =185.2 Hz And the corresponding coherence time can be approximately obtained by [19]

$$T_c \approx \frac{9}{16\pi f_m} \tag{4.28}$$

where f_m is the maximum Doppler shift given by $f_m = v/\lambda$. This yields T_c = 966.788 us

Coherence time is actually a statistical measure of the time duration over which the channel impulse response is essentially invariant, and quantifies the similarity of the chan-

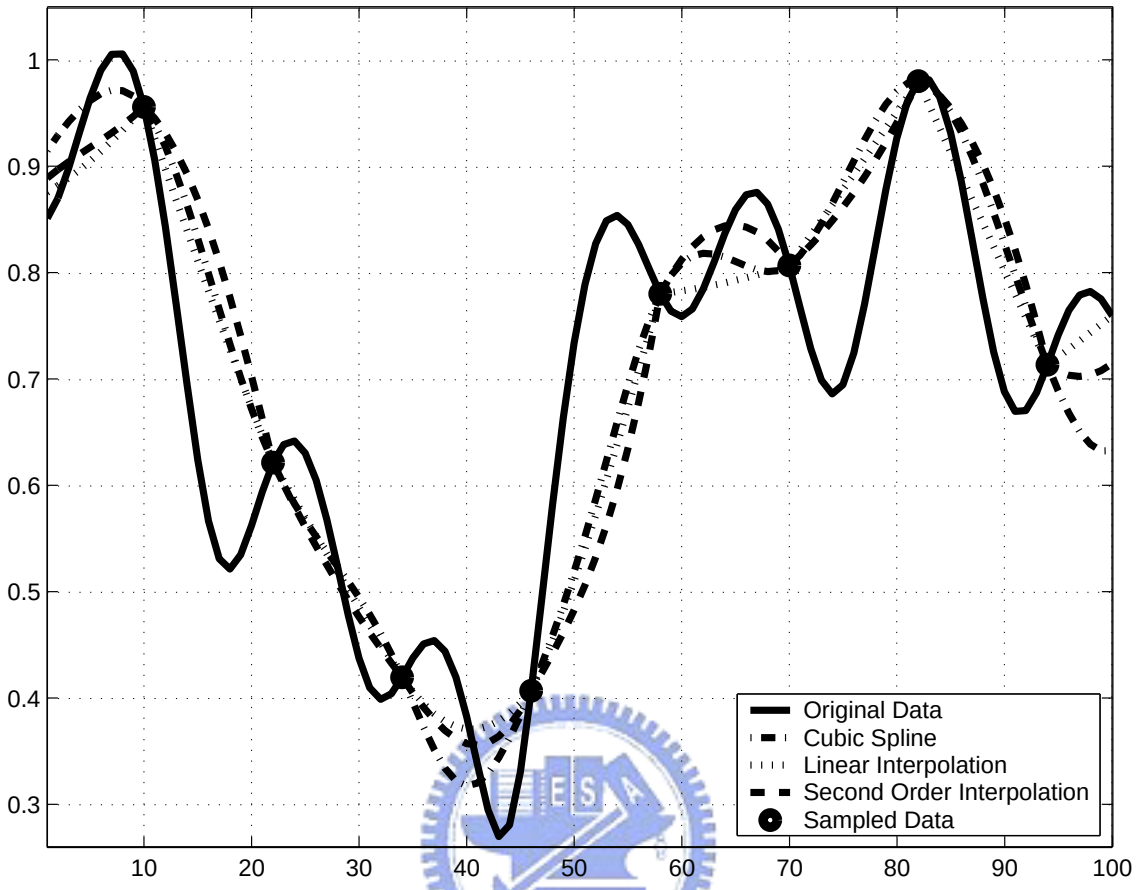

Fig. 4.1: The result of different interpolation methods.

nel resonse at different times. As this OFDMA system is operated with a data bandwidth equals 10 MHz, the symbol period time is then $(2048 + 256)/10M$ = 201.9 μs (with a CP rate of $1/8$). And the channel can be seen as a slow fading one if the coherence time is greater than the symbol period. The channel impulse response changes at a rate much slower than the transmitted baseband signal $s(t)$ in a slow fading channel. In this case, the channel may be assumed to be static over one or several reciprocal bandwidth intervals.

Following the calculations above, the channel response over $\frac{966.788}{201.9} = 4.788$ symbols is assumed to be static. Thus we use an averaging methods over 5 symbols to reduce the noise term as

$$\tilde{h}_a(f) = \frac{\tilde{h}_0^{interp}(f) + \tilde{h}_{-1}^{interp}(f) + \tilde{h}_{-2}^{interp}(f) + \tilde{h}_{-3}^{interp}(f) + \tilde{h}_{-4}^{interp}(f)}{5} \tag{4.29}$$

where $\tilde{h}_a(f)$ is the estimated channel after the moving average and $\tilde{h}_{-n}^{interp}(f)$, n=1$\cdots$4 is the interpolated channel response at nth previous symbol time.

4.3.2 Exponential average

The OFDM system can be described as

$$\mathbf{Y} = \mathbf{H} \cdot \mathbf{X} + \mathbf{N} \tag{4.30}$$

where **Y** is the received symbol, **H** is the channel response, **X** is the transmitted symbol, and **N** is the complex additive white Gaussian noise with variance σ_m^2. If X_p is a pilot subcarrier, the instantaneous channel estimate is obtained as

$$\hat{\mathbf{X}}_{p,LS} = \frac{\mathbf{Y}_p}{\mathbf{X}_p} = \mathbf{H}_p + \frac{\mathbf{N}_p}{\mathbf{X}_p} \tag{4.31}$$

Because the noise term **N** is the complex additive white gaussian noise whose mean is 0. If the channel **H** remains static, compared with the former method to take five symbols to do the averaging, the more symbols we take, the more we can eliminate the noise term. However, the more symbols we take, the more complicated the hardware is, since we have to use more registers to store the estimated channel responses. Thus we think of a alogorithm to use all the former symbols without store them. It is the simple exponential averaging as follows:

$$\tilde{h}_n^{exp}(f) = \begin{cases} \omega \cdot \tilde{h}_{n-1}^{exp}(f) + (1-\omega) \cdot \tilde{h}_n^{interp}(f), & n > 1, \\ \tilde{h}_n^{interp}(f), & n = 1, \end{cases} \tag{4.32}$$

where $\tilde{h}_n^{exp}(f)$ is the estimated channel after using this method at nth symbol time, $\tilde{h}_n^{interp}(f)$ is the channel response by using only interpolations discussed before at nth symbol time, and ω is the weighting of the $\tilde{h}_{n-1}^{exp}(f)$, likewise, the weighting of $\tilde{h}_n^{interp}(f)$ is $(1-\omega)$.

The performance is better than the moving averaging one in static channel simulation. But the channel varies in the mobile transmission, the estimation brought all the former information may not be suitable in this situation. The data and the different weighting ω comparison will be given in the next chapter.

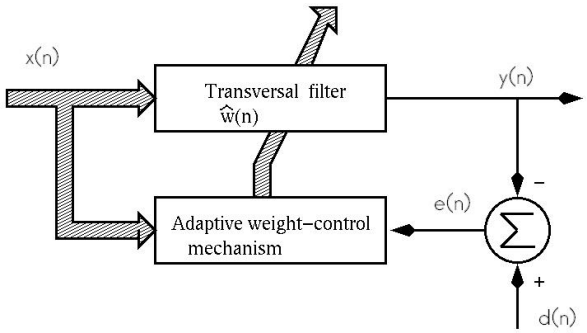

Fig. 4.2: Block diagram of adaptive transversal filter.

4.3.3 LMS adaptation

The LMS algorithm [20] is a linear adaptive filtering algorithm, which in general, consists of two basic processes:

- **A filtering process**

  The filter process involves (i) computing the output of a linear filter in response to an input signal and (ii) generating an estimation error by comparing this output with a desired response.

- **An adaptive process**

  The process involves the automatic adjustment of the parameters of the filter in accordance with the estimation error.

The combination of these two processes working together constitutes a feedback loop, as illustrated in the block diagram of Fig. 4.2. First, we have a transversal filter, around which the LMS algorithm is built, and this component is responsible for performing the filtering process. Second, we have a mechanism for performing the adaptive control process on the tap weights of the transversal filter, hence the designation $adaptive\ weight-control\ mechanism$ in the figure.

The LMS adaptation algorithm equations has been broadly known and used:

- **Filtering:**

$$y(n) = \mathbf{w}^H(n)\mathbf{x}(n) \tag{4.33}$$

- **Error estimation:**

$$e(n) = d(n) - y(n) \tag{4.34}$$

- **Tap-weight vector adaptation:**

$$\mathbf{w}(n+1) = \mathbf{w}(n) + 2\mu\mathbf{e}^*(n)\mathbf{x}(n) \tag{4.35}$$

The equations above derive a set of tap-weight vector $\mathbf{w}(n)$, which can be used to multiply another value to do the adaptation. Thus we could use the equations to do like an equalizer, that is, we multiply the recived data by the tap-weight vector. Because the tap-weight vector obtained is the information of the equalizer, which needs to be inversed to get the estimated channel, we try to use the LMS adaptation scheme to estimate the channel frequence response directly. Eq. (4.34) and the cost function in square error sence can be rewritten as

$$\mathbf{e}(n) = \mathbf{d}(n) - \mathbf{w}^H(n)\mathbf{x}(n), \tag{4.36}$$

$$\hat{\xi}(n) = \mathbf{e}^2(n) = |\mathbf{d}(n) - \mathbf{w}^H(n)\mathbf{x}(n)|^2. \tag{4.37}$$

To do the LMS estimation on the channel directly, we have a new error definition $\varepsilon(n)$ and its corresponding cost function:

$$\varepsilon(n) = \mathbf{x}(n) - \mathbf{w}^H(n)\mathbf{d}(n), \tag{4.38}$$

$$\hat{\xi}_\varepsilon(n) = \varepsilon^2(n) = |\mathbf{x}(n) - \mathbf{w}^H(n)\mathbf{d}(n)|^2. \tag{4.39}$$

Thus the adaptive equation becomes

$$\mathbf{w}(n+1) = \mathbf{w}(n) + 2\mu\varepsilon(n)^*\mathbf{d}(n). \tag{4.40}$$

To use the same denotions as they are in the previous sections, we rewrite (4.39) as:

$$\hat{\xi}_\varepsilon(n) = \varepsilon^2(n) = |\mathbf{Y}(n) - \hat{\mathbf{H}}^H_{p,LMS}(n)\mathbf{X}(n)|^2. \tag{4.41}$$

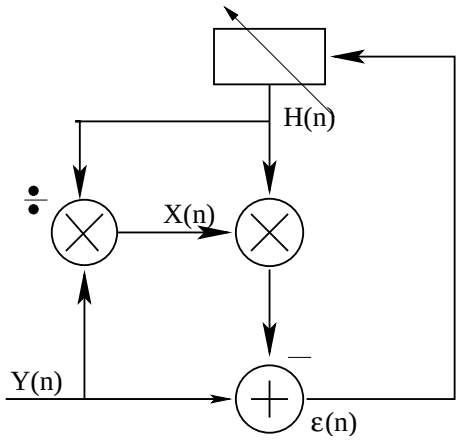

Fig. 4.3: Illustration of LMS adaption for channel estimation.

and (4.40) as:

$$\hat{\mathbf{H}}_{p,LMS}(n+1) = \hat{\mathbf{H}}_{p,LMS}(n) + 2\mu\varepsilon(n)^{*}\mathbf{X}(n). \tag{4.42}$$

The **X**(n) is obtained by assuming our estimation is perfect then **X**(n)=$\frac{\mathbf{Y}(n)}{\hat{\mathbf{H}}_{p,LMS}(n)}$. This adaptation algorithm is shown as Fig. (4.3)

In our simulation, we use the interpolated channel estimation as the $\hat{\mathbf{H}}_{p,LMS}(0)$, the $\hat{\mathbf{H}}_{p,LMS}(n)$ is obtained by (4.42) when $n > 1$. Following the algorithm, only the first symbol pilot information is used in the whole flow, thus the pilot information of other symbols is wasted. Therefore, we try to combine the interpolated channel and the $\hat{\mathbf{H}}_{p,LMS}(n)$ which is the estimated channel by using LMS algorithm when $n > 1$. The equation of this combination can be given as

$$\tilde{h}_n^{ModifiedLms}(f) = \begin{cases} \alpha \cdot \tilde{h}_n^{p,LMS}(f) + (1-\alpha) \cdot \tilde{h}_n^{iterp}(f), & n > 1, \\ \tilde{h}_n^{interp}(f), & n = 1, \end{cases} \tag{4.43}$$

where $\tilde{h}_n^{p,LMS}(f)$ is the channel estimated by the LMS adaptation algorithm with the $\hat{\mathbf{H}}_{p,LMS}(n-1)$ and it is also denoted as $\hat{\mathbf{H}}_{p,LMS}(n)$, and $\tilde{h}_n^{iterp}(f)$ is the channel estimated by interpolation. The α and the $(1-\alpha)$ is the weighting factor for $\tilde{h}_n^{p,LMS}(f)$ and $\tilde{h}_n^{iterp}(f)$.

4.3.4 Two-Dimensional interpolation

Let us review the downlink variable pilot allocation of IEEE 802.16a in Fig. 3.2. And the equation of the allocation formula is again

$$varLocPilot_k = 3L + 12P_k \tag{4.44}$$

where:

- $varLocPilot_k$ = carrier index of a variable-location pilot
- $L \in 0, \cdots, 3$ is a function of the symbol index, modulo 4
- $P_k \in \{0, 1, 2, \cdots, N_{varLocPilots} - 1\}$

Because the position of the variable location pilots varies with a period of four symbols, we could use the variable location pilots at the other three symbols. The maxmimun number of the variable location pilots we can use is

$$(N_{varLocPilots} - N_{CoincidentPilots}) \times 4 + N_{fixLocPilots} = (142 - 8) \times 4 + 32 = 568 \tag{4.45}$$

where the $N_{ConincidentPilots}$ is the number of the variable location pilots which are coincident with the fix location pilots. Thus we can use the extrapolation in the time domain to estimate the channel frequency response on the variable location pilots of other symbols. This method is illustrated in Fig. 4.4. And the mathematical expression is

$$\begin{aligned}\tilde{h}^{2D-extrap-p}(f) = \quad & \tilde{h}^p_0(f) + (\tilde{h}^p_{-1}(f) - \tilde{h}^p_{-5}(f))\tfrac{5}{4} + \tilde{h}^p_{-5}(f) \\ & + (\tilde{h}^p_{-2}(f) - \tilde{h}^p_{-6}(f))\tfrac{6}{4} + \tilde{h}^p_{-6}(f) + (\tilde{h}^p_{-3}(f) - \tilde{h}^p_{-7}(f))\tfrac{7}{4} + \tilde{h}^p_{-7}(f),\end{aligned} \tag{4.46}$$

where $\tilde{h}^p_{-n}(f)$ for $n = 0, 1, \cdots, 7$ is the channel frequency response of pilot carriers in the nth previous symbol time. We can use interpolations again on the frequency domain after knowing $\tilde{h}^{2D-extrap-p}(f)$. Since the number of the pilots becomes $568/166 = 3.421$ times compared with the original case, the better estimation is obtained.

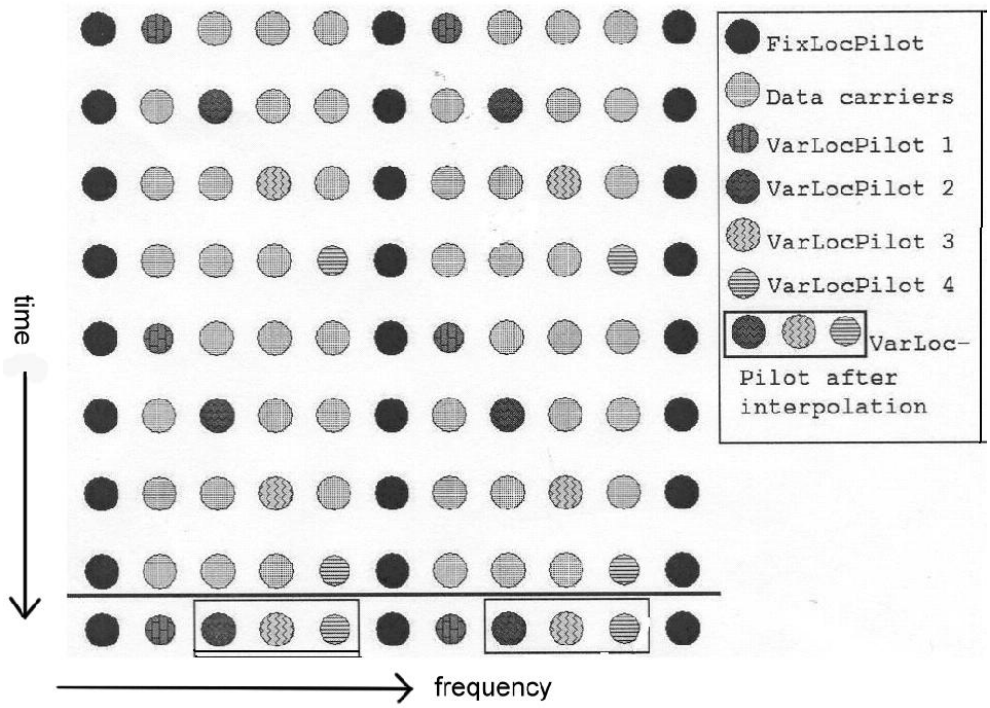

Fig. 4.4: Illustration of the 2-D interpolation scheme.

However, there are extra seven registers needed to store the channel frequency response on pilot carriers. Except for the hardware concern, the fast fading channel might seriously effect the accuracy of the interpolations on the time domain. Because we need to use the information before seven symbols, the channel may have changed a lot during this period of time. Thus, we can use less variable location pilots in previous symbols which means only 1 or 2 more sets of variable location pilots are taken. Eq. (4.46) becomes

$$\begin{aligned}\tilde{h}^{2D-extrap-p}(f) = \quad & \tilde{h}^{p}_{0}(f) + (\tilde{h}^{p}_{-1}(f) - \tilde{h}^{p}_{-5}(f))\tfrac{5}{4} + \tilde{h}^{p}_{-5}(f) \\ & + (\tilde{h}^{p}_{-2}(f) - \tilde{h}^{p}_{-6}(f))\tfrac{6}{4} + \tilde{h}^{p}_{-6}(f),\end{aligned} \tag{4.47}$$

and

$$\tilde{h}^{2D-extrap-p}(f) = \tilde{h}^{p}_{0}(f) + (\tilde{h}^{p}_{-1}(f) - \tilde{h}^{p}_{-5}(f))\frac{5}{4} + \tilde{h}^{p}_{-5}(f). \tag{4.48}$$

Comparison of these three equations will be discussed in the next chapter.

Chapter 5

Simulation Study

The flow of our simulations is as shown in Fig. 5.1. We assume to have perfect synchronization since the aim is to observe channel estimation performance.

After doing channel estimation, we can calculate the channel MSE which is mean square error between the real channel and the estimated one. We can also obtain the SER, the symbol error rate, after demapping. The mapping here is based on the 16QAM, thus the E_b/N_0 is $SNR/4$. And the constellation of the 16-QAM modulation is introduced before in Fig. 3.3. The static channel and the Rayleigh fading channel as well are simulated and discussed in this chapter.

Before simulating on multipath channel, we do the simulation with an AWGN channel which means we transmit the data through a one-path channel with $h[0] = 1$, and then add AWGN noise on it. The result is shown in Fig. 5.2, and is almost the same with the

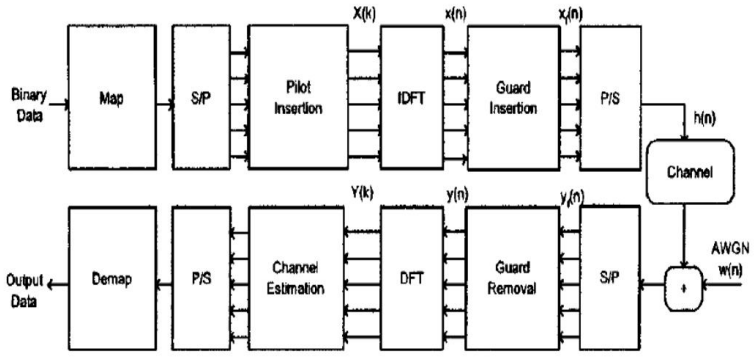

Fig. 5.1: The flow chart of the simulations.

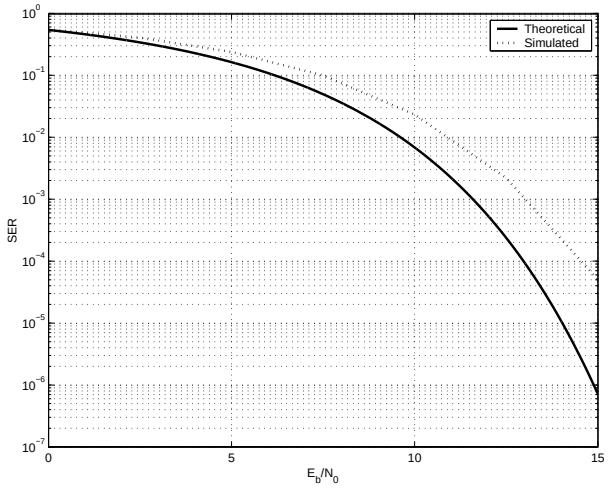

Fig. 5.2: The simulation result on AWGN channel.

Table 5.1: Channel Impulse Response

Tap	Delay (OFDM samples)	Amplitude	Amplitude (in dB)
1	0	1	0
2	2	0.3162	-5
3	17	0.1995	-7
4	36	0.1296	-8.87
5	75	0.1	-10
6	137	0.1	-10

theoretical one.

5.1 Channel model

A multipath fading channel models are used in the simulations. Since the specifications IEEE 802.16a did not assign a mobile channel model, we thus refer the channel in the [1]. The channel model is the ATTC (Advanced Television Technology Center) and the Grande Alliance DTV Laboratory's ensemble E model. Its static impulse response is given in Table 5.1.

Table 5.2: Interpolation Errors

	Linear Interpolation	**Second-Order Interpolation**	**Cubic Spline**
Theoretical	0.0254	0.0330	0.0285
Simulation Result	0.0208	0.0269	0.0237

5.2 Definitions of SER and channel MSE

The SER in the below simulations is denoted for the average symbol error rate at the specific E_b/N_0. Likewise, the MSE is denoted for the average $|\hat{h} - h|^2$ at the E_b/N_0. The averages in above sentences are in the subcarriers senses.

5.3 Simulations on Static (Stationary) Channels

We use the static case of the channel model introduced before to be our static simulation model.

5.3.1 Comparison of interpolation methods

First we want to discuss the error caused by the interpolation scheme. Thus we let the data transmit after the channel without adding noise, using the information on the pilot carriers to get the channel frequency response by doing the interpolation. Then we calculated the average $|\hat{x}_i - x_i|^2$ on each subcarrier by simulating 10000 symbols. The theoretical symbol error rate with Gaussian noise power N_0 for M-ary QAM can be obtained by [19]

$$P_e = 4(1 - \frac{1}{\sqrt{M}})Q(\sqrt{\frac{3NE_b}{(M-1)N_0}}) \tag{5.1}$$

where $N = \log_2 M$ and we have $N = 4$ with $M = 16$ here. The E_b is $E_s/4$ and the E_s is normalized to be 1 in our simulation. If we subtitude $|\hat{x}_i - x_i|^2$ for N_0, we can get a theoretical symbol error rate and is given in Table 5.2. We can observe that, the simulated symbol error rate differs from the theoretical one. Therefore, the interpolation error can not be considered Gaussian noise.

Fig. 5.3 shows the result of different interpolations in MSE and SER senses. Out of our expection, as shown in the figure, the linear interpolation has a better performace than the others. That might be owing to the lack of pilot carriers. That is, the carrier spacing is too large for we to use the pilot carriers which outside the two adjacent ones.

There are also error floors in all the three interpolations. As we discussed in the previous chapter, the pilot carriers are insuffecient of this six taps channel. There is a great improvement in the 2-D interpolation simulation in this aspect. Since we have almost four times the number of pilot carriers in the 2-D interpolation simulation. The second-order interpolation outperforms the linear one. And the larger the E_b/N_0 is, the better the second-order interpolation performs than the linear one. The detail and the result will be discussed also in the section of the subsection 5.1.5.

5.3.2 Result of moving averaging

Because there is no parameter needed to be adjudged in this scheme. We put the result and the the analysis in the section 5.2.6.

5.3.3 Comparison of different weightings in exponential averaging

In this simulation, we use only linear interpolation because of the result of the former section. For the linear interpolation performs better than the second-order one with limited pilot carriers number.

We can see from Fig. 5.4, the MSE gets smaller when ω increases from 0 to 0.9. But the MSE gets larger when $\omega > 0.9$, thus the best choise of ω is 0.9. There is a gain about 8 dB when $\omega = 0.9$ compared with using only linear interpolation. In the circuit realization concern, we might chose $(1-\omega)$ as $(\frac{1}{2})^n$ which can easily done by right shift the data.

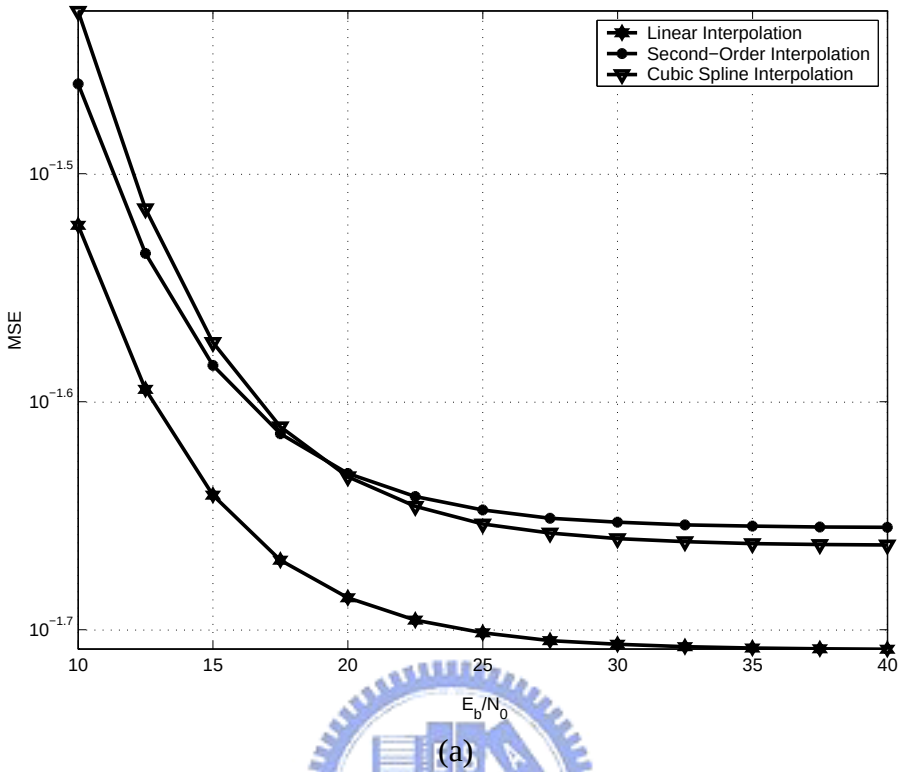

(a)

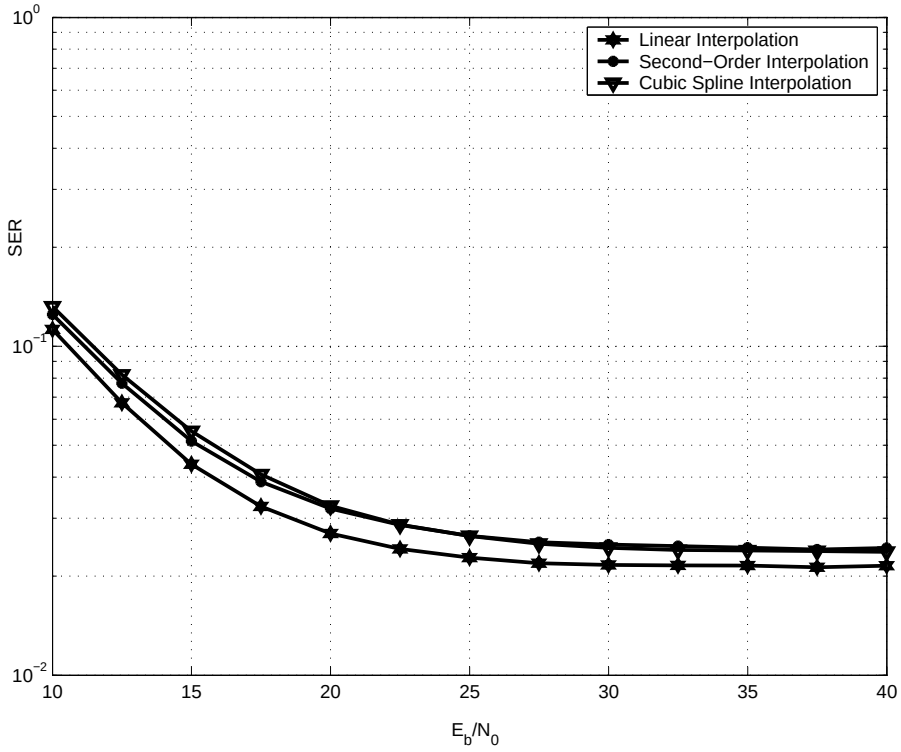

(b)

Fig. 5.3: The (a) MSE and (b) SER of diffrent interpolation schemes.

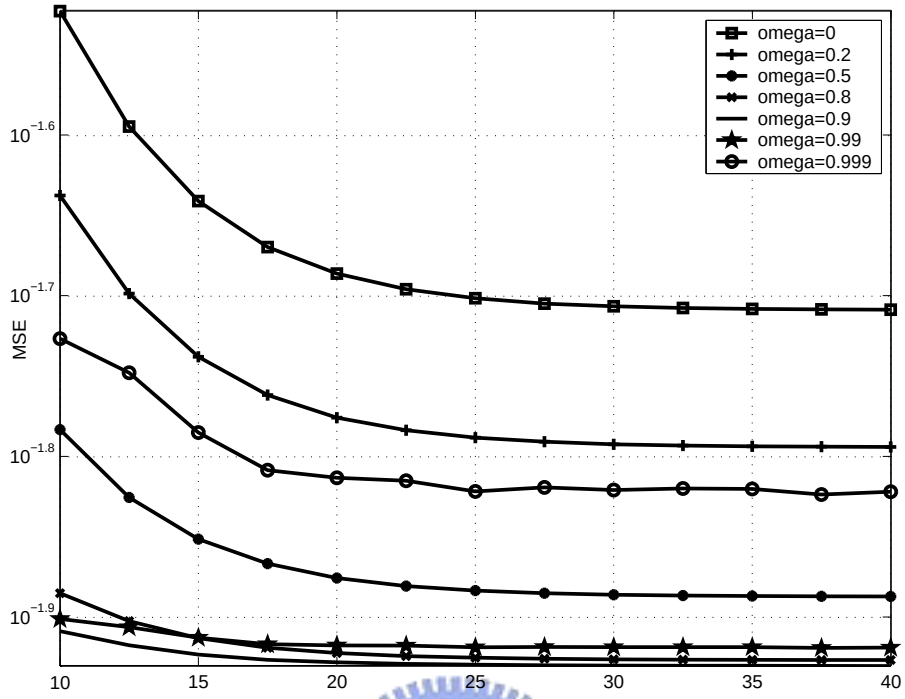

(a)

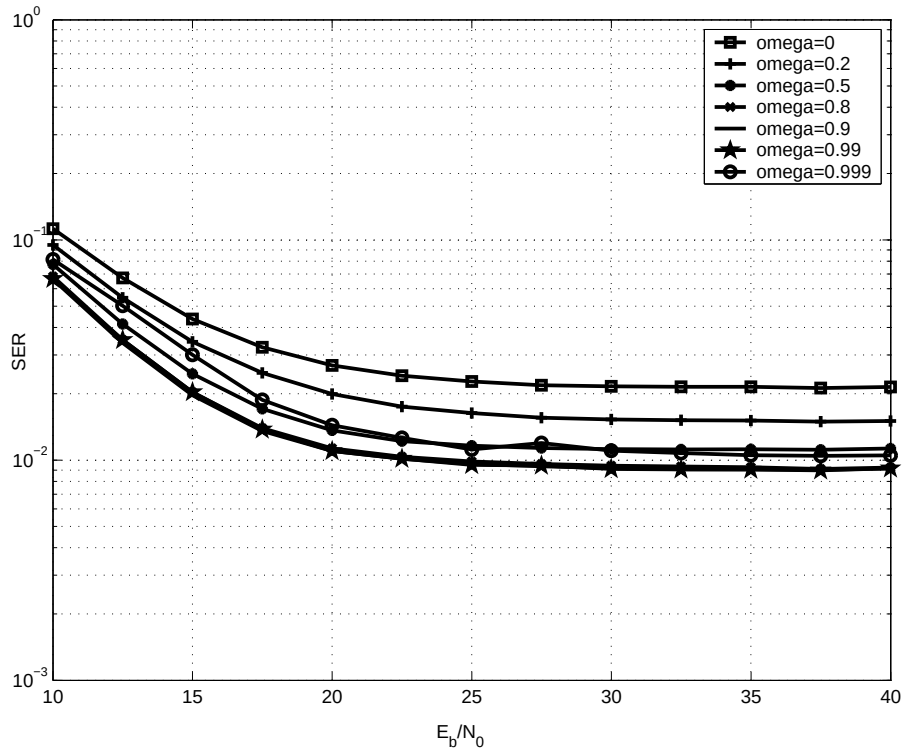

(b)

Fig. 5.4: The (a) MSE and (b) SER of using different weightings in exponential averaging.

5.3.4 Comparison of different weightings in LMS adaptation method

Obeying the criterion of the step-size parameter μ of the LMS algorithm [20], [21]:

$$0 < \mu < \frac{1}{3tr[\mathbf{R}]}, \tag{5.2}$$

where tr[**R**] is the sum of the powers of the signal samples at the filter tap inputs, which is the powers of the channel impulse response in our case. And the tr[**R**] equals 1.1766, thus we choice μ to be 0.05 and 0.005. Recalling the adaptive equation $\hat{\mathbf{H}}_{p,LMS}(n+1) = \hat{\mathbf{H}}_{p,LMS}(n) + 2\mu\varepsilon(n)^*\mathbf{X}(n)$, the **X**(n) here is obtained by the decision output which is decided by the receive data over estimated channel, which **X**(n)=$\frac{\mathbf{Y}(n)}{\hat{\mathbf{H}}_{p,LMS}(n)}$. And this is based on the assumption that our decision is correct. We also compare the different weighting α of the LMS filter output and the interpolated data. The result is shown in Fig. 5.5.

5.3.5 Comparison of the sets of variable location pilots taken in the 2-D interpolation

Because we need to use the information of previous seven symbols. We do the 2-D interpolation after the 8th symbol. The previous seven symbols are estimated simply with 1-D interpolation.

The result of the 2-D interpolation with using different sets of variable location pilots is shown in Fig. 5.6. We can observe that, the second-order interpolation performs better than the linear one while the variable location pilots and the E_b/N_0 increase. For example, with four sets of variable location pilots are taken, there is a better performance in the second-order interpolation when $E_b/N_0 > 25$dB. This observation also provides the reason why the linear interpolation has a better performance than the second-order and cubic spline ones. It is because the lack of pilot carriers which is allocated and arranged with the IEEE 802.16a specifications.

Note that there are also error floors in these simulations. That is because we use 1-D interpolation at the first seven symbols. The summation of the symbol errors of the seven

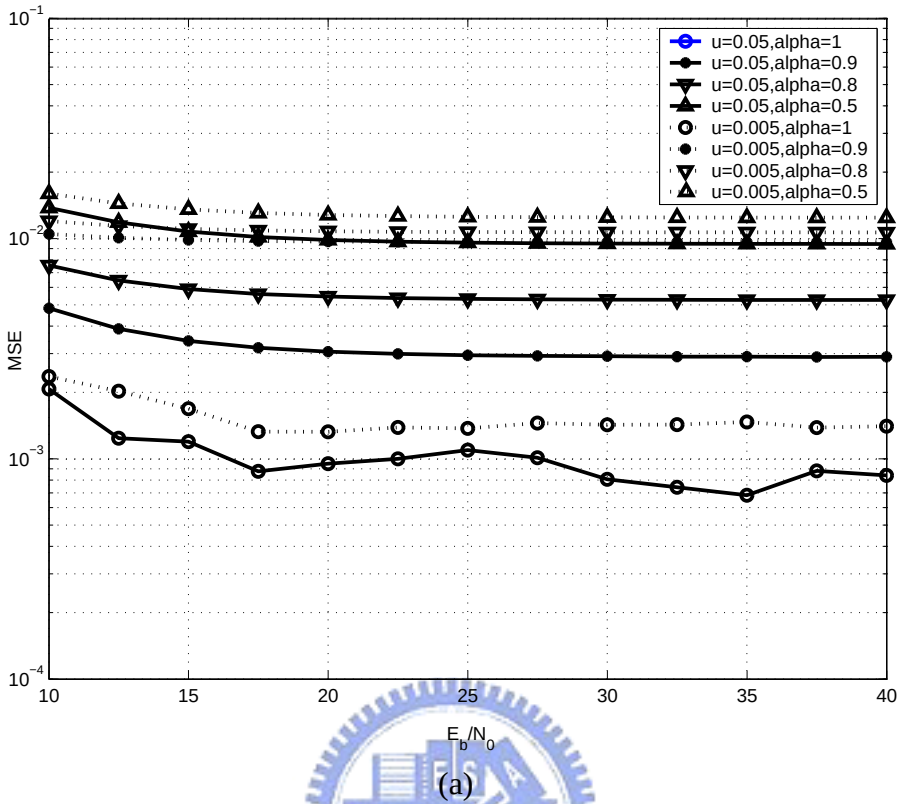

(a)

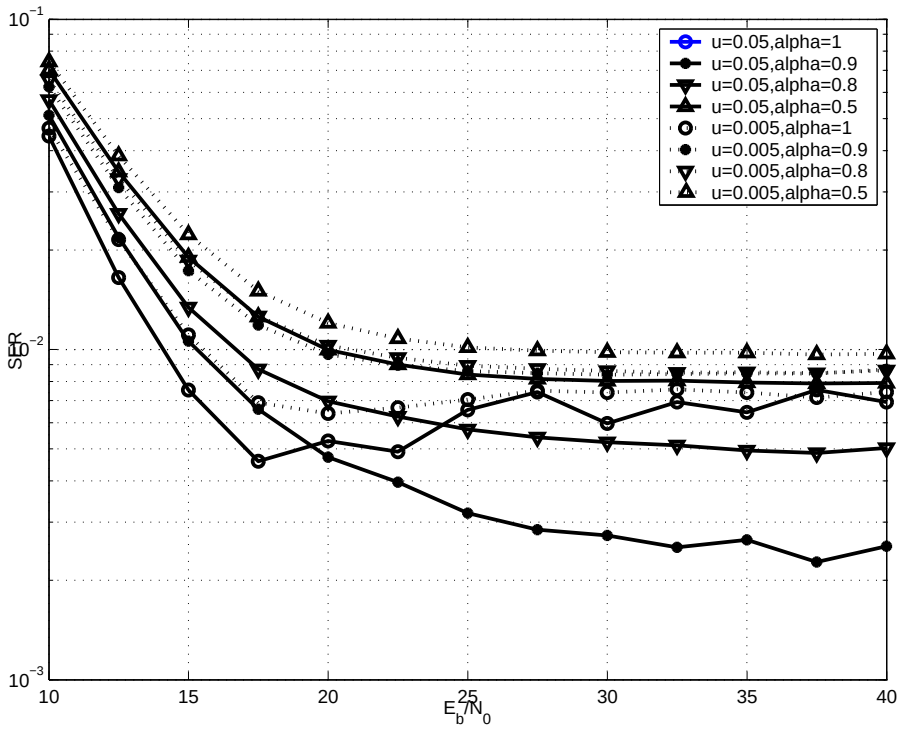

(b)

Fig. 5.5: The (a) MSE and (b) SER for different weightings and different step-size parameters in LMS method.

symbols dominate while there are almost no errors after the 8th symbol. Thus we can conclude that, the more symbol we count to calculate the symbol error rate, the smaller the value is.

5.3.6 Comparison of all the methods of time domain improvement

Overall MSE and SER

First, we would like to compare the overall MSE and SER of the methods discussed before. For our convenience, we chose the best one in each time domain improvement scheme to be compared, $\omega = 0.9$ in the exponential average, $\alpha = 1$ in the LMS adaptaion, and four sets of variable location pilots in 2-D interpolation.

As shown in Fig. 5.7, the performace of time domain improvement techniques from worst to best are linear interpolation without doing any improvement scheme, moving average, exponential average, 2-D interpolation and the LMS adaptaion. Note that, the 2-D interpolation method outperform the LMS adaptation one only when the $E_b/N_0 > 24$dB. And every time domain improvement in this comparison is done with linear interpolation in the frequency domain, except for the 2-D interpolation which is done with second-order one.

Convergence rate

Except for the MSE and SER, we also care about the convergence rate of each time domain improvement methods. The overall simulation result is calculated by doing 1000 symbols per E_b/N_0. But the actual data frame might not consist of so many symbols, thus we need to know the decrease rate of MSE and SER in time domain if there is any.

We can observe from the Fig. 5.8, the decrease rate of LMS with $\alpha = 0.5$ is the largest among all at the beginning when $E_b/N_0 = 15$ dB as well as $E_b/N_0 = 30$ dB. But the convergence value of MSE of LMS adaptation when $E_b/N_0 = 15$ dB and of 2-D interpolation with second-order interpolation at frequency domain when $E_b/N_0 = 30$ dB is the smallest. For saving the hardware complexity, we can use LMS adaptation with

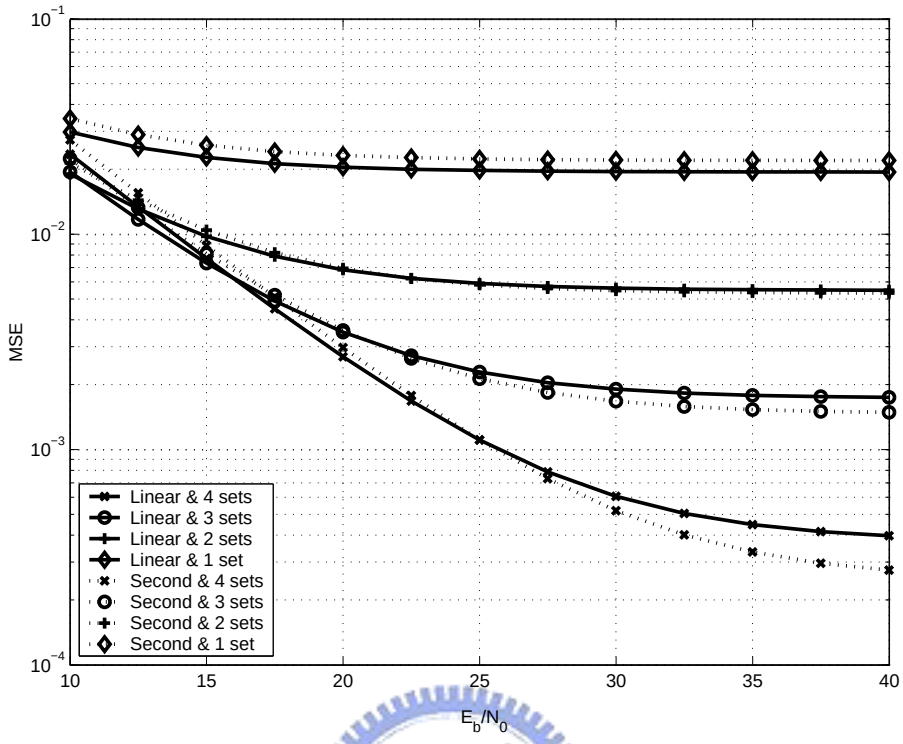

(a)

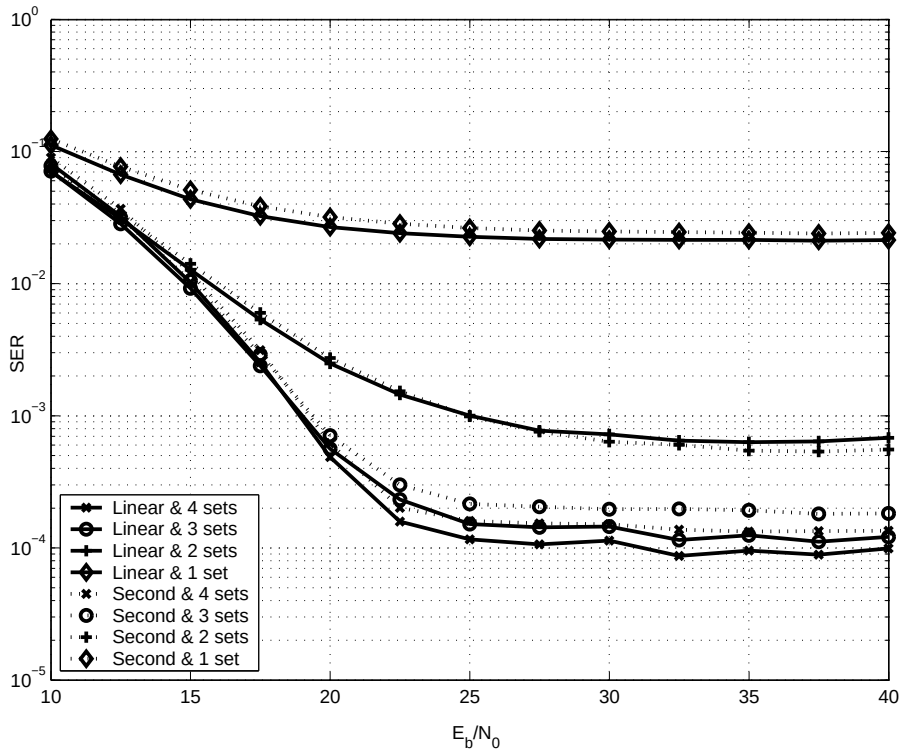

(b)

Fig. 5.6: The (a) MSE and (b) SER of the 2-D interpolation with different sets of variable location pilots and different interpolation schemes on frequency domain.

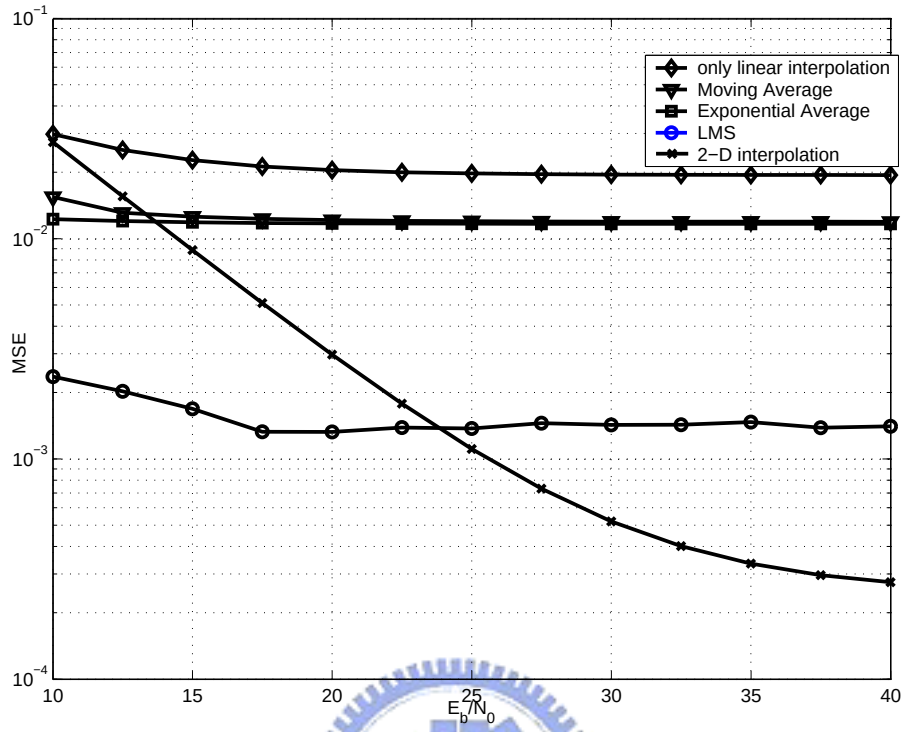

(a)

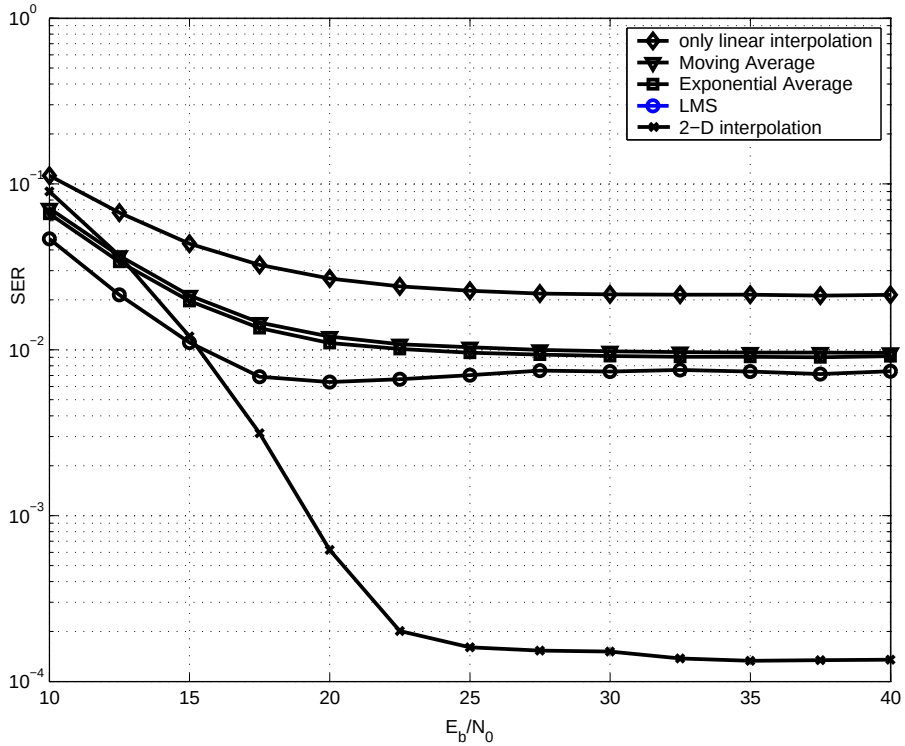

(b)

Fig. 5.7: The (a) MSE and (b) SER of all the time domain improvement methods.

$\alpha = 0.5$ at the first five symbols and LMS adaptation with $\alpha = 1$ at the latter symbols. And we can get a decent solution of every symbol by using the similar hardware structure.

Complexity

The complexity of the four time domain improvement techniques is compared in Table 5.3.

5.3.7 The relation of channel MSE and SER

We try to find and explain the relation of simulated symbol error rates with their corresponding channel mean square error. First, we explored if the channel mean square error is ralated to the data mean square error or not, or equivalently if $|\hat{x}-x|^2 \propto |\hat{h}-h|^2$. If we can find the relation between them, then we can use the (5.1) to calculated the theoretical symbol error rate with $N_0 = |\hat{x} - x|^2$.

We try to obtain the relation between channel MSE and SER in linear interpolation simulation. Before finding the relation, we try to substitude the $E|\hat{x} - x|^2$ of each subcarrier for N_0 in the (5.1) to obtain the theoretical SER of each subcarrier,or equivalenty SER_i. Then we calculte the $E|SER_i|$ to be compared with the simulated SER. The comparison is shown in Table 5.4. Because there is slight diference of the theoretical SER and the simulated one, we could assume the $E|\hat{x} - x|^2$ is Gaussian distributed.

Assume there is no AWGN noise, then

$$\begin{aligned} E|\hat{x} - x|^2 = &\quad E|\tfrac{y}{\hat{h}} - x|^2 = E|\tfrac{x\cdot h}{\hat{h}} - \tfrac{x\cdot\hat{h}}{\hat{h}}|^2 \\ = &\quad E|x|^2 E|\tfrac{h-\hat{h}}{\hat{h}}|^2 = E|\tfrac{h-\hat{h}}{\hat{h}}|^2. \end{aligned} \tag{5.3}$$

If $E|h - \hat{h}|^2$ is independent with $E|\hat{h}|^2$, then the equation above can be rewritten as

$$\frac{E|\hat{x} - x|^2}{E|\hat{h} - h|^2} = E|\frac{1}{\hat{h}}|^2. \tag{5.4}$$

Substituding $E|\frac{1}{\hat{h}}|^2$ with $E|\frac{1}{h}|^2$ in (5.4), then we illustrate $\frac{E|\hat{x}-x|^2}{E|\hat{h}-h|^2}$ and $E|\frac{1}{\hat{h}}|^2$ in the Fig.(5.9) when SNR=40dB (thus we can assume there is no AWGN). We can find that $\frac{E|\hat{x}-x|^2}{E|\hat{h}-h|^2}$ is

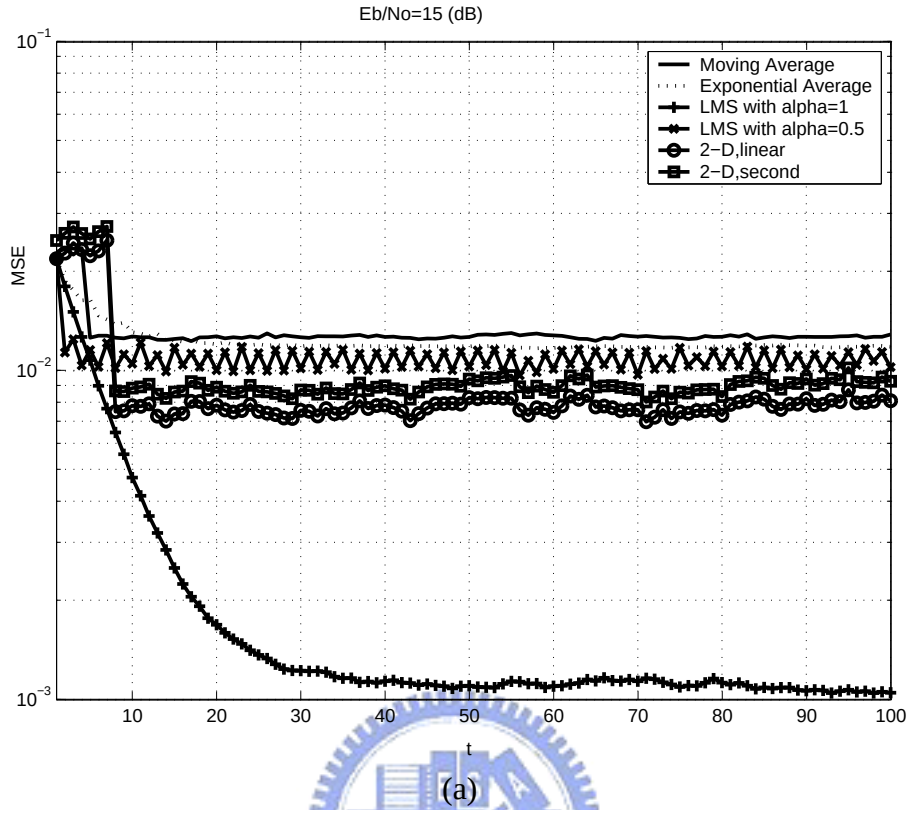

(a)

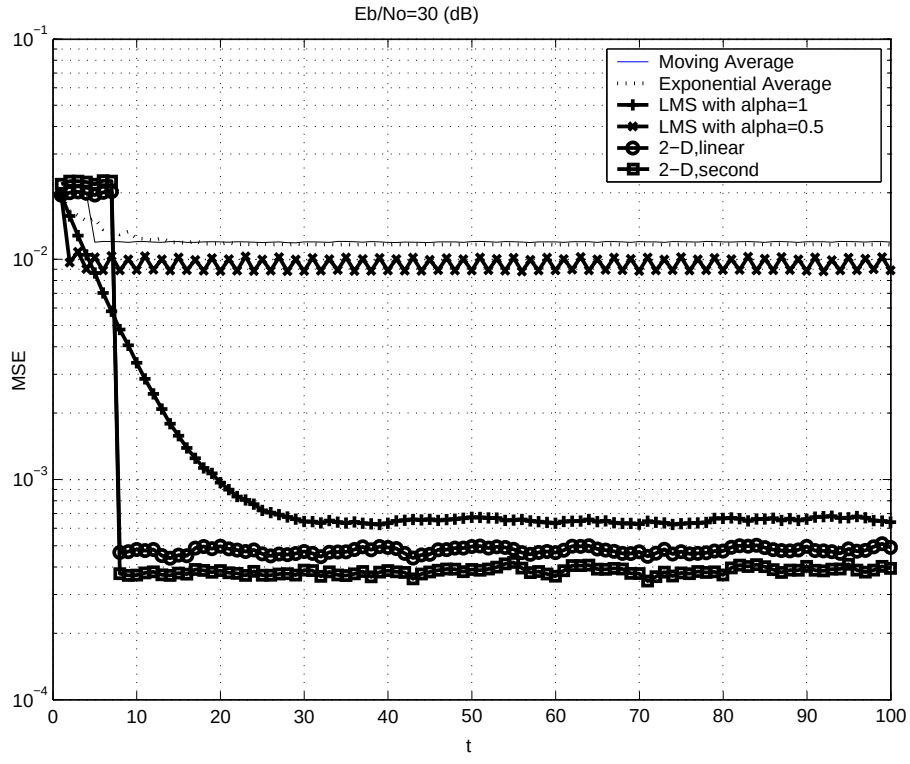

(b)

Fig. 5.8: The MSE of all the time domain improvement methods when (a) $E_b/N_0 = 15(dB)$ (b) and $E_b/N_0 = 30(dB)$.

Table 5.3: Comparison of Computation Complexities and Extra Registers of Several Time Domain Improvement Techniques

Time Domain Improvement schemes	**Computation Complexity**	**Extra Registers**
Moving Average	1MPY + 4Adds	4
Exponential Average	2MPYs + 2Adds	1
LMS Adaptation	4MPYs + 1Add	1
2-D Interpolation (four sets of varLocPilots)	3MPYs + 6Adds	7

Table 5.4: The Theoretical SER and the Simulated One in Linear Interpolation

E_b/N_0 **(in dB)**	**Theoretical**	**Simulated**
10	0.1217	0.1141
20	0.0321	0.0289
30	0.0260	0.0223

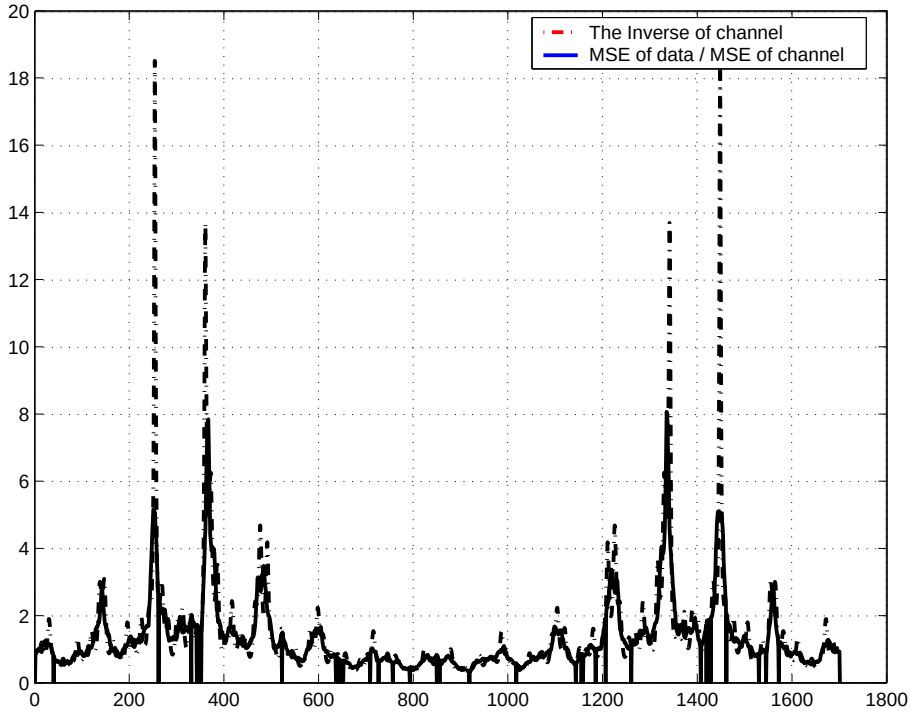

Fig. 5.9: The data MSE and channel MSE versus each subcarrier in the linear interpolation case when SNR=40dB.

very similar to $E|\frac{1}{\hat{h}}|^2$, thus the independency exists. Therefore, $E|\hat{x}-x|^2$ is in proportion to $E|\hat{h}-h|^2$ with a vector $E|\frac{1}{\hat{h}}|^2$, or equivalently $E|\frac{1}{h}|^2$. If we know the $E|\hat{h}-h|^2$, then

we can calculate the $E|\hat{x}-x|^2$, and the theoretical SER can be obtained in consequence.

Note that, there are points whose value are zero in the line $\frac{E|\hat{x}-x|^2}{E|\hat{h}-h|^2}$. That is because the subcarriers at that points are fix location pilots and the $E|\hat{x}-x|^2$ at those points are always zero.

5.4 Simulations of Fading Channels

We use block type Rayleigh fading as our fading channel. And the parameters of Rayleigh fading are obtained as [22]. It is an improved Jakes' simulation model and the below equations are its mathematical expressions.

$$R(t) = R_c(t) + jR_s(t), \tag{5.5}$$

$$R_c(t) = \frac{2}{\sqrt{M}} \sum_{n=1}^{M} \cos(\psi_n) \cdot \cos(w_d t \cdot \cos\alpha_n + \phi), \tag{5.6}$$

$$R_s(t) = \frac{2}{\sqrt{M}} \sum_{n=1}^{M} \sin(\psi_n) \cdot \cos(w_d t \cdot \cos\alpha_n + \phi), \tag{5.7}$$

where

$$\alpha_n = \frac{2\pi n - \pi + \theta}{4M}, \quad n = 1, 2, \cdots, M, \tag{5.8}$$

where θ, ϕ, and ψ_n are statistically independent and uniformly distributed over $[-\pi, \pi)$ for all n, and $M = 8$ in our simulation.

The Rayleigh fading channel is created following the equation:

$$h[n] = \sum_{i=1}^{i=k} R_i[n] \times \alpha_i \delta[n - d_i]; \quad H(f) = FFT\{h[n]\} \tag{5.9}$$

where k is the total path number, α_i is the static power of the ith path, $R_i[n]$ is the Rayleigh parameter calculated by (5.5), and the d_i is the delay spread of the ith path. Because we simulate the data after channel by $Y(f) = X(f) \times H(f) + N$, therefore we have to transform $h[n]$ to the frequency domain. In Rayleigh channel simulation, the $R_i[n]$ varies every symbol, thus we need to do the FFT comutation every symbol. To reduce the complexity and the computation time, we simplify (5.9) into these two:

$$Base_i(f) = FFT\{\alpha_i \delta[n - d_i]\}, \tag{5.10}$$

$$H(f) = \sum_{i=1}^{i=k} R_i[n] \times Base_i(f). \tag{5.11}$$

Then we compute FFT only one time at the first, and the latter channel frequency response can be obtained by the linear operation of the summation of the product of Rayleigh parameter and the $Base_i(f)$.

5.4.1 Comparisons of All Methods of Time Domain Improvement

After simulating our methods on Raleigh fading channel, the LMS adaptation and the exponential average schemes do not perform as well as they do in static channels. Therefore, we take the two methods and the moving average one as well to compare together. The comparison of the three algorithm is show in Fig. 5.10.

The SER of LMS adaptaion with α=1 even amounts to $15/16$, which is the same as guessing the result. That is because the LMS adaptation method uses the pilot information only at the first symbol, and the step-size parameter in LMS adaptation may not be large enough to correct the error caused by the fading channel. The performace improves much when α=0.5 and 0.2 individually. And the main problem of the exponential average method is that we take all ther former symbols to eliminate the noise term. However, the change in the channel frequency response may cause larger error than the eliminated noise term. Since the downlink frame is composed of $3 \times N$ symbols where N is a postive integer, we could reset the data in the register every six symbols, and the (4.32) then becomes

$$\tilde{h}_n^{all}(f) = \begin{cases} \omega \cdot \tilde{h}_{n-1}^{all}(f) + (1-\omega) \cdot \tilde{h}_n(f), & n_{mod(6)} = 1, 2, \cdots, 5, \\ = \tilde{h}_n(f), & n_{mod(6)} = 1, \end{cases} \tag{5.12}$$

where $n_{mod(6)}$ is the remainder in dividing n by 6. The result of exponential average method with ω=0.2 and 0.5, with and without reset are also shown in Fig. 5.10 and the performance is almost the same. When we use the reset strategy also in the LMS adaptation algorithm, and the result improves.

The moving average scheme, however, does not have a good outcome as we expected.

Though we calculated the coherence time to be 966.788 us with the center frequency f_c=2 GHz, and the channel can be assumed to be static during five symbol times, the simulation of doing average with the data of five symbols did not improve as much as we thought.

The 2-D interpolation has the best performance among all the time domain interpolation methods. As in the case of static channels, the four sets of variable location pilots with second-order interpolation in the frequency domain gives the least SER in Fig. 5.11. In Fig. 5.11, the line marked "ideal" refers to the ideal case when we know the exact channel frequency response. Thus the symbol errors come only from the additive noise. And the performance difference between the best one among all, which is the four sets variable location pilots with second-order interplation, and the ideal case is about 2.5 dB when the velocity of the receiver is 27 km/h and is about 5 dB when the velocity is 54 km/h.

But there is a shortcome of 2-D interpolation. As we mentioned in the static channel simulation, we needed seven symbols to get enough information for 2-D interpolation. In the first seven symbols, the channel estimation is done by only 1-D interpolation. Thus we can use two kinds of strategies for the first seven symbols and the latter ones seperately.

Note there is also an error floor when the E_b/N_0 increases. This is due to the change in the channel frequency response dominates the noise term and therefore, even though the noise decreases, the value of the symbol error rate still remains unreduced.

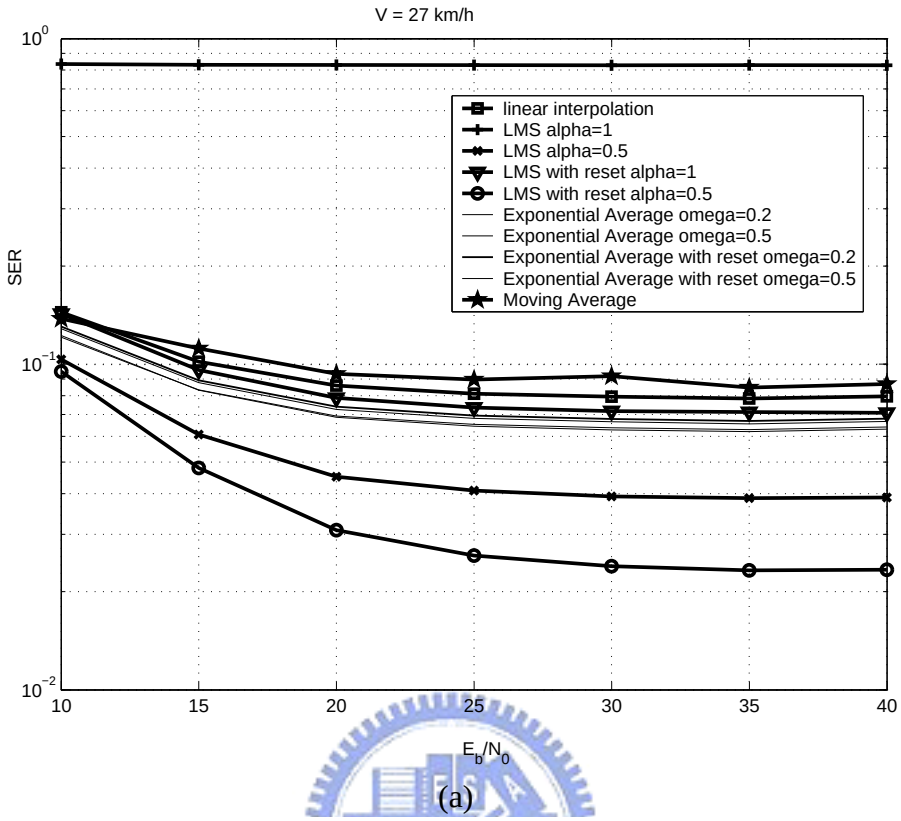

(a)

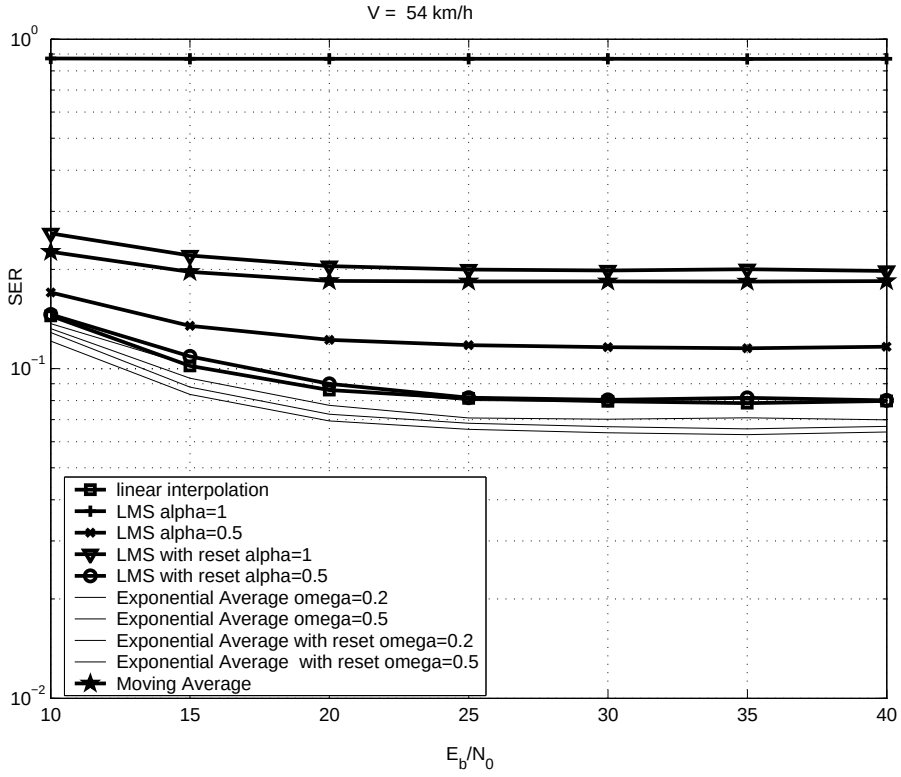

(b)

Fig. 5.10: The SER of the LMS and average all the former algorithm when V= (a) 27 km/h and (b) 54 km/h.

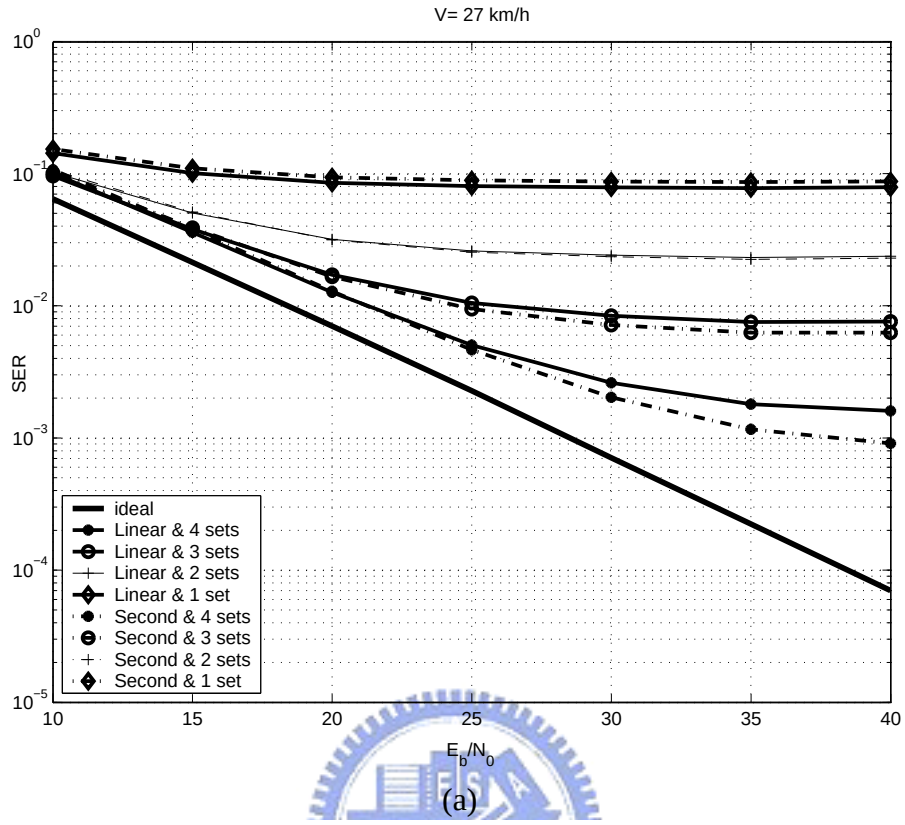

(a)

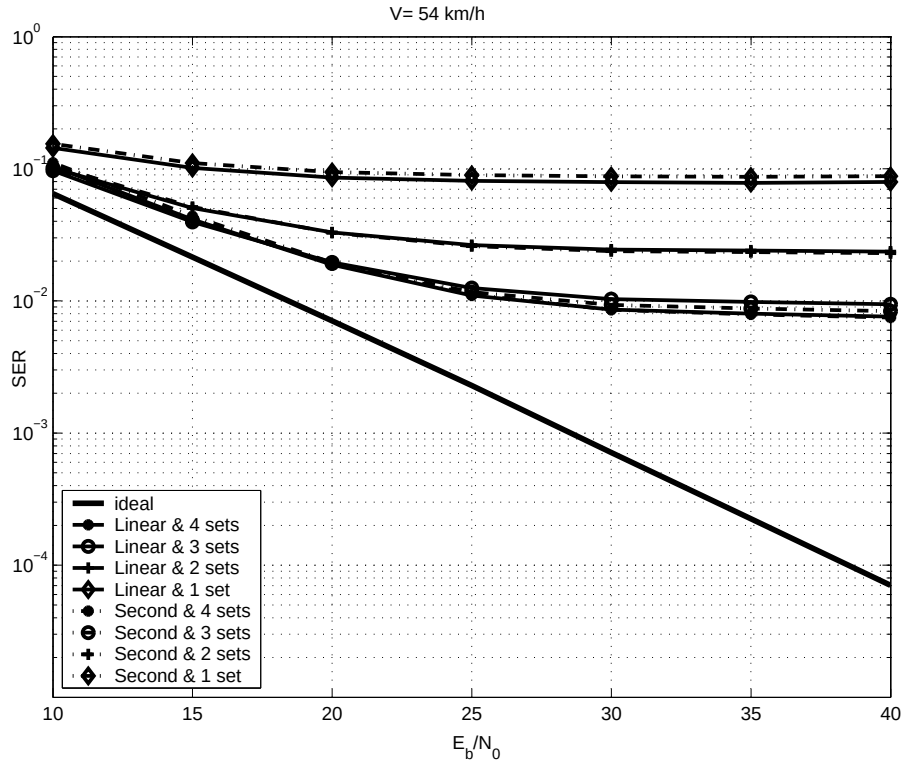

(b)

Fig. 5.11: The SER of the 2-D interpolation when V = (a) 27 km/h and (b) 54 km/h.

Chapter 6

Conclusion and Future Work

6.1 Conclusion

To do the downlink channel estimation in IEEE 802.16a, we got three main points: first, we had to use the pilot carriers to estimate the channel frequency response on the pilot subcarriers. Second, the interpolations are needed to estimate the channel frequency response on the rest subcarriers. And the third point was to obtain a better estimation by time domain improvement schemes.

We used LS estimator instead of the LMMSE one not only for the complexity concern but also dued to the unknown statistical properties of channels. And the three kind of interpolation were compared, linear, second-order, and the cubic spline interpolation. The four kind of time-domain improvement schemes were moving average, exponential average, the LMS adaptation and the 2-D interpolation.

Out of our expectation, the estimation errors of different interpolations from large to small were cubic spline, second-order, and linear. After doing the 2-D interpolation, the number of pilot carrier increased, and the second-order interpolation started to outperform the linear one as E_b/N_0 grows. Therefore, not only the E_b/N_0 but also the pilot spacing mattered for the efficiency of the interpolation.

We also found that, although we calculated the coherence time to be $966.788us$ with the center frequency f_c=2 GHz, and the channel could be assumed to be static during five symbol times. The simulation of doing moving average with the data of five symbols did

not improve as much as we thought.

The 2-D interpolation of four sets of variable location pilots showed the best performance, but there were extra three multipliers, six adders and seven registers. And the computation complexity was the highest among all. With second-order interpolation, the 2-D interpolation had even a better result. However, to do the 2-D interpolation, there were seven symbols needed to be stored for enough information. The square error between the estimated and the origin channl of the former seven symbols could affect the overall MSE much. For the data stream was not large, this error may dominate the outcome thus an error floor. Regardless the hardware complexity, we could use another structure and algorithm at the beginning to obtain the optimum performance and result.

6.2 Future Work

We may put our emphasis on the DSP implementation as well as better estimations in the future. And the task includes the following part:

- Explore new methods to resist the fading channel at high speed of receivers.
- Use better interpolation to solve the problem of lack of pilot carriers.
- Develop a better scheme to do the interpolation on time domain (for the 2-D interpolation aspect).
- Revise the data type from floating to fixed.
- Reduce the complexity and try to excute the program real time.
- Using the proporties of the DSP board to do the optimization.

We also need to modify the I/O interface to casecade our channel estimation block with other functions to accomplish our final project such as synchronization, channel coding, source coding$\cdots$, etc.

Bibliography

[1] S. Coleri, M. Ergen, A. Puri, and A. Bahai, "Channel estimation techniques based on pilot arrangement in OFDM systems," *IEEE Trans. Broadcasting*, vol. 48, no. 3, pp. 223–229, Sep. 2002.

[2] ETSI, *Radio Broadcasting Systems: Digital Audio Broadcasting to Mobile, Portable and Fixed Receivers*. European Telecommunication Standard ETS 300-401, Feb. 1995.

[3] ETSI, *Digital Video Broadcasting: Framing Structure, Channel Coding, and Modulation for Digital Terrestial Television.*, European Telecommunication Standard EN 300-744, Aug. 1997.

[4] IEEE Std 802.16a-2003, *IEEE Standard for Local and Metropolitan Area Networks — Part 16: Air Interface for Fixed Broadband Wireless Access Systems — Amendment 2: Medium Access Control Modifications and Additional Physical Layer Specifications for 2–11GHz.* New York: IEEE, April 1, 2003.

[5] R. van Nee and R. Prasad, *OFDM for Wireless Multimedia Communications.* Boston: Artech House, 2000.

[6] D. Matiae, "OFDM as a possible modulation technique for multimedia application in the range of mm waves, "http://www.ubicom.tudelft.nl/MMC/Docs/introOFDM.pdf.

[7] O. Edfors, M. Sandell, J. J. van de Beek, D. Landstrom, and F. Sjoberg, "An introduction to orthogonal frequency-dicision multiplexing," http://courses.ece.uiuc.edu/ece459/spring02/ofdmtutorial.pdf.

[8] J. A. C. Bingham, "Multicarrier modulation for data transmission: an idea whose time has come," *IEEE Commun. Mag.*, vol. 28, no. 5, pp. 5–14, May 1990.

[9] http://WirelessMan.org/pub/backgrounder.html.

[10] http://www.intel.com/update/contents/st08031.htm.

[11] http://wirelessman.org/tga.

[12] M.-H. Hsieh, "Synchronization and channel estimation techniques for OFDM systems," Ph.D. thesis, Department of Electronics Engineering, National Chiao Tung University, Hsinchu, Taiwan, R.O.C., May 1998.

[13] O. Edfors, M. Sandell, J. J. van de Beek, S.K. Wilson, and P.O. Börjesson, "OFDM channel estimation by singular value decomposition," in. *IEEE 46th Vehicular Technology Conference*, Atlanta, GA, USA, Apr. 1996, pp. 923–927.

[14] C. K. Koc and G. Chen, "Authors' reply [Computational complexity of matrix inversion]," *IEEE Trans. Aerospace Electronic Systems*, vol. 30, no 4, p. 1115. Oct. 1994.

[15] M.-H. Hsieh and C.-H Wei, "Channel estimation for OFDM systems based on comb-type pilot arrangement in frequency selective fading channels," *IEEE Trans. Consumer Electron.* vol. 44, no. 1, pp. 217–225, Feb. 1998.

[16] S. G. Kang, Y. M. Ha and E. K. Joo, "A comparative investigation on channel estimation algorithms for OFDM in mobile communications," *IEEE Trans. Broadcasting*, vol. 49, no. 2, pp. 142–149, June 2003.

[17] S. A. Dyer and J. S. Dyer, “Cubic-spline interpolation. 1,” *IEEE Instrument. Measurement Mag.*, vol. 4, no. 1, pp. 44–46, Mar. 2001.

[18] S. A. Dyer and H. Xin, “Cubic-spline interpolation. 2,” *IEEE Instrument. Measurement Mag.*, vol. 4, no. 2, pp. 34–36, June 2001.

[19] T. S. Rappaport, *Wireless Communications Principles and Practice.* Upper Saddle River, New Jersey: Prentice Hall, 1996.

[20] S. Haykin, *Adaptive Filter Theory.* Upper Saddle River, New Jersey: Prentice Hall, 2002.

[21] B. F. Boroujeny, *Adaptive Filters Theory and Applications.* West Sussex, England: Wiley, 1999.

[22] Y. R. Zheng and C. Xiao, “Simulation models with correct statistical properties for Rayleigh fading channels,” *IEEE Trans. Commun.*, vol. 51, no. 6, pp. 920–928, June 2003.

作者簡歷

陳盈縈，民國六十九年生於台北市。民國九十一年畢業於國立交通大學電子工程學系，同年進入國立交通大學電子研究所，從事通訊系統相關研究。民國九十三年取得碩士學位，論文題目為「IEEE 802.16a 分時雙工正交分頻多重進接之下行通道估測之研究與技術」。研究興趣為通訊系統及數位訊號處理。